Feasibility of Large-Scale Ocean CO_2 Sequestration

Annual Report 2006

Start Date: October 1, 2005

End Date: September 30, 2006

Principal Author(s): Peter G. Brewer

Issued: December 2006

DoE Award Number: DE-FC26-00NT40929

Submitting Organization: Monterey Bay Aquarium Research Institute
7700 Sandholdt Road
Moss Landing, CA 95039

ABSTRACT
This report covers research accomplished during CY 2006 under a modification of a previous award. During this period we completed analysis of the acoustic detection and modeling of a rising deep-sea liquid CO_2 plume, and published the results in a major journal. The results are applicable to detection of leakage of CO_2 from the sea floor, either from natural CO_2 vents, or from purposefully disposed CO_2 in sub-sea geologic formations.

In April 2006 we executed, in collaboration with colleagues from Massachusetts Institute of Technology, Oak Ridge National Laboratory, and Canada a novel at sea experiment on the creation of a sinking plume of a CO_2 hydrate composite paste, extruded through nozzles designed by ORNL. The work showed that a sinking, and slowly dissolving, mass can be created at depths where the pure liquid (above) would rise far and fast. In August 2006 we executed a cruise to the massive exposed methane hydrates in Barkley Canyon, off-shore Vancouver Island. There we cored the exposed hydrates, and exposed the specimens on the sea floor at 850m depth to liquid CO_2 in a 3 liter closed container. The object was to examine possible inter-conversion of methane hydrate to CO_2 hydrate with liberation of methane gas, and sequestration of the CO_2 as a solid. Each of these complex experiments was successfully executed and the results reported in major journals and/or at national meetings.

TABLE OF CONTENTS

INTRODUCTION

The research described here is the result of a scientific odyssey, begun at a turbulent time when the description of a possible solution to the sequestration of fossil fuel CO2 included direct disposal by injection into the deep ocean. First described as a possibility a quarter of a century ago the subject matter existed only in cartoon form for many years. This was fundamentally changed by the simple and direct execution of small-scale ROV deployed experiments that clearly revealed the role of the formation and dissolution of hydrates (Brewer et al., 1999) in the deep sea that were the object of much speculation. The cartoon sketches (eg. Hanisch, 1988) showed multiple possibilities – formation of a rising plume of liquid CO2, a sinking plume of liquid CO2, formation of a sinking hydrate mass, "permanent" storage as a hydrate, and formation of a "lake" of CO2 on the sea floor. Over the last few years we have set ourselves the discipline of testing each of these concepts with economy and skill. The scale has been small, the environmental impacts negligible, and the scientific output large.

In the present report we address two of these topics – observation in real time and modeling of a freely rising plume of liquid CO2 within the hydrate phase regime, and amazingly formation within the very same depth regime of a sinking plume of CO2 created by an injection nozzle that forces the vigorous intermixing of sea water and CO2 in the desired 6:1 ratio at the fine droplet scale.

The deliberate injection of very large quantities of CO2 into the ocean water column is unlikely to occur because of environmental concerns, and because of London Convention challenges, but nonetheless it has been extensively reviewed as Chapter 6 of the 2005 IPCC Special Report on Carbon Capture and Storage, where work supported under this award was highlighted. But this field is still of compelling national and international interest for at least three reasons:

i) The possible leakage from CO2 stored in sub-sea geologic formations, its detection and fate, and the degree to which natural liquid CO2 vents can be used as useful analogs.

ii) The "active" injection of fossil fuel CO2 is a theoretical possibility. The very real "passive" invasion of fossil fuel CO2 into the ocean has now surpassed 500 billion tons, and is proceeding at ~ 1 million tons CO2 per hour, with significant ocean acidification occurring today. This only-slightly-indirect injection demands study, and has vastly greater environmental and geopolitical implications than any possible engineering solution.

iii) CO2 sequestration is expensive, and much has been made of the combination of CO2 injection with the recovery of coal bed methane. The ocean equivalent of this may well be the injection of CO2 into a methane hydrate formation, with the possible formation of free methane gas, and the storage of CO2 as a solid hydrate. This field is now in the ferment of early research and is in great need of clarity and scientific discipline.

EXECUTIVE SUMMARY

This report covers research accomplished during CY 2006 under a modification of a previous award. During this period we completed analysis of the acoustic detection and modeling of a rising deep-sea liquid CO_2 plume, and published the results in a major journal. The results are applicable to detection of leakage of CO_2 from the sea floor, either from natural CO_2 vents, or from purposefully disposed CO_2 in sub-sea geologic formations. The plume analysis agreed closely with numerical models. In addition the well-known use of acoustics to detect marine organisms offers a useful future application for the assessment of marine biologic impacts of such CO_2 leakage.

In April 2006 we executed, in collaboration with colleagues from Massachusetts Institute of Technology, Oak Ridge National Laboratory, and Canada a novel at sea experiment on the creation of a sinking plume of a CO_2 hydrate composite paste, extruded through nozzles designed by ORNL. The work showed that a sinking, and slowly dissolving, mass can be created at depths where the pure liquid would rise far and fast. Imaging of the plume revealed fine details of nozzle design effects, and well established sinking rates and lifetimes for the extruded material.

In August 2006 we executed a cruise to the massive exposed methane hydrates in Barkley Canyon, off-shore Vancouver Island. There we cored the exposed hydrates, and exposed the specimens on the sea floor at 850m depth to liquid CO_2 in a 3 liter closed container. The object was to examine possible inter-conversion of methane hydrate to CO_2 hydrate with liberation of methane gas, and sequestration of the CO_2 as a solid. We investigated the course of the reaction by in situ laser Raman spectroscopy, successfully scanning a complex multi-phase system in three dimensions with sub-millimeter precision half a mile below the sea surface! Although only 48 hours was available for this experiment results clearly showed that the complex inter-conversion was indeed initiated, and all critical chemical phases were detected in the system.

EXPERIMENTAL

This report covers essentially three separate experiments. Each one has a specific protocol. This is covered in the individual reports presented as Appendices here.

RESULTS AND DISCUSSION

The results and discussion for each experiment are reported in separate files in the Appendix.

CONCLUSION

The research supported here shows that it is possible, with economy and skill, to advance knowledge of the role of the ocean in either active or passive CO2 sequestration with small-scale experiments that have minimal environmental impact; by doing so we rid society of wrong ideas and imaginary problems, and highlight real issues and valid solutions. The simple and direct acoustic detection of CO2 leakage and the fate of a rising CO2 plume elegantly solves a controversial issue. The formation of a composite paste of CO2 hydrate which creates a sinking plume within the very same depth regime that the free liquid will rise sheds light on the fate of CO2 hydrate and helps solve a challenge put forward in the important PCAST report on the future of fossil energy. By devising new means of investigating the possible inter-conversion of methane hydrate for CO2 hydrate

we have for the first time taken to the field a complex and controversial subject that has hitherto been explored only in small laboratory pressure cells.

REFERENCES

Brewer, P.G., G. Friederich, E.T. Peltzer, and F.M. Orr, Jr. (1999) Direct Experiments on the Ocean Disposal of Fossil Fuel CO_2. *Science*, **284**, 943-945.

Hanisch, C. (1998) *Environ. Sci. Technol.*, **32**, 20A-24A.

APPENDICES

Three-dimensional acoustic monitoring and modeling of a deep-sea CO_2 droplet cloud

Peter G. Brewer,[1] Baixin Chen,[2] Robert Warzinki,[3] Arthur Baggeroer,[4] Edward T. Peltzer,[1] Rachel M. Dunk,[1] and Peter Walz[1]

Received 26 June 2006; revised 7 August 2006; accepted 20 October 2006; published 8 December 2006.

[1] We show that release of 5 liters of liquid CO_2 at 1000 m depth can be readily detected acoustically, and tracked for over 30 minutes, and 150 m of ascent, with both surface ship (38 kHz) and ROV (675 kHz) sonars. The released liquid broke up into droplets covered with a hydrate film. The remarkably sensitive acoustic response of the droplets may be attributed to the high sound speed contrast between CO_2 (300 m/sec) and sea water (1500 m/sec), the near spherical shape of the droplets created by the hydrate shell, and the high compressibility of the liquid. The observed cloud conformed closely to models of CO_2 disposal, allowing for reasonable predictions of larger scale processes. This offers a remarkably sensitive technique for examination in real time of engineered releases of CO_2, volcanic sea floor liquid CO_2 plumes, or leakage from geologic CO_2 storage. **Citation:** Brewer, P. G., B. Chen, R. Warzinki, A. Baggeroer, E. T. Peltzer, R. M. Dunk, and P. Walz (2006), Three-dimensional acoustic monitoring and modeling of a deep-sea CO_2 droplet cloud, *Geophys. Res. Lett.*, *33*, L23607, doi:10.1029/2006GL027181.

1. Introduction

[2] Scientific and public attitudes towards the role of the ocean in taking up fossil fuel CO_2 are confused. It has been recognized for decades that the ocean, through its alkalinity, "acts as a giant regulator of carbon dioxide" [*Callendar*, 1938]; the surface ocean now absorbs 30% of all fossil fuel CO_2 emissions [*Sabine et al.*, 2004], and the accumulated fossil fuel CO_2 burden is now about 500 Gt CO_2. Without the benefit of massive absorption of this artifact of mankind's energy use the world would face an insurmountable atmospheric CO_2 problem. Ocean uptake of fossil fuel CO_2 by the surface ocean has therefore typically been described as a beneficial natural process, quite distinct from the possible direct injection of CO_2 into oceanic deep waters as a means of CO_2 sequestration [*Brewer et al.*, 1999; *Intergovernmental Panel on Climate Change* (*IPCC*), 2005], with concerns over environmental harm [*Seibel and Walsh*, 2001]. So strong has been the divide that while terrestrial CO_2 enrichment experiments releasing up to 10^3 tons CO_2/year routinely take place [*DeLucia et al.*, 1999], oceanic experiments with the release of only a few kilograms of CO_2 have been subject to enormous scrutiny, yet there are compelling needs for carrying out a wide variety of such experiments.

[3] With the belated recognition that the scale of surface ocean CO_2 invasion is now so large that changes in sea water pH of 0.3 or more are predicted to occur by mid-century [*Brewer*, 1997; *Caldeira and Wickett*, 2003], the lines between so called "passive" and possible "direct" introduction of CO_2 to the ocean have become blurred. Stabilization of atmospheric CO_2 levels at 550 ppmv is often mentioned as a desirable policy goal, and emission trajectories for achieving this have been described [*Wigley et al.*, 1996]. Yet this implies at equilibrium the transfer of some 6 trillion tons of CO_2 to the ocean over the course of several centuries [*IPCC*, 2005]. The consequences of this for marine ecosystems are largely unknown [*Cicerone et al.*, 2004; *Royal Society*, 2005], but are generally expected to be negative [*Portner et al.*, 2004]. While simple aquarium studies can shed some light on potential impacts, open ecosystem perturbation studies will also be required.

[4] Here we describe advances in one such experimental technique, that of observing a freely released CO_2 cloud, such as might occur from engineered releases of CO_2 directly into the deep ocean, leakage of CO_2 from sub-sea floor geologic disposal sites, or from natural vents.

[5] Liquid CO_2 is a highly compressible fluid, with the property of being less dense than sea water at depths less than $\sim$2500 m, and more dense at greater depths. Thus gravitationally stable pools of liquid CO_2 may be placed on the deep sea floor for experimental purposes [*Brewer et al.*, 1999], and these have been used to investigate the perturbed pH field and biological responses around an experimental site [*Barry et al.*, 2004]. Equivalent experiments in shallower waters, where CO_2 forms a rising cloud, have been considered very difficult to execute and plans for medium scale experiments have lead to controversy [*Figueiredo et al.*, 2003]. Yet it is this scenario that is of great interest, for it simulates the release of liquid CO_2 from volcanic sites [*Sakai et al.*, 1990; *Lupton et al.*, 2006] and relates to possible leakage of CO_2 from sub-seafloor geological storage sites. The assessment of ocean ecosystem impacts at such sites has recently been identified by the International Energy Agency's Greenhouse Gas Programme as requiring a critical study.

[6] The difficulty of observing a freely released rising CO_2 cloud is such that only very small scale observations of individual rising droplets [*Brewer et al.*, 2002] have been reported so far. These few observations have been used as input for sophisticated models [*Alendal and*

[1]Monterey Bay Aquarium Research Institute, Moss Landing, California, USA.
[2]National Institute of Advanced Industrial Science and Technology, Tsukuba, Japan.
[3]National Energy Technology Laboratory, U.S. Department of Energy, Pittsburgh, Pennsylvania, USA.
[4]Department of Ocean and Electrical Engineering, Massachusetts Institute of Technology, Cambridge, Massachusetts, USA.

0094-8276/06/2006GL027181$05.00

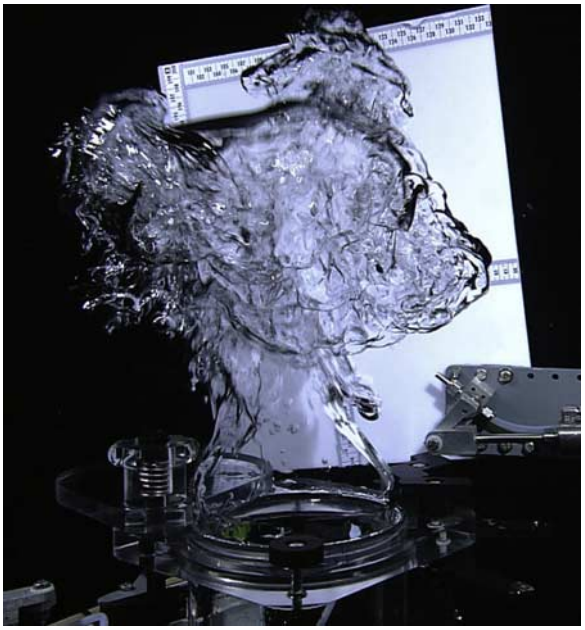

Figure 1. Image of the 1025 m ~ 5 L liquid CO_2 experiment at the moment of release. The container volume is 7.5 L, diameter is 15 cm. The white panel with the scale is for size estimation and to provide visual contrast for imaging the transparent fluid. Immediately after release the buoyant liquid begins to break down into small ~ cm size globules due to Taylor instabilities. The ensemble of droplets of varying sizes ascends as a dissolving complex cloud, with the rise rate of individual droplets depending upon size, and the changing density with the surrounding sea water.

Drange, 2001; *Chen et al.*, 2003; *Sato*, 2004; *Gangstø et al.*, 2005] of larger scale CO_2 clouds, but no observational constraints have yet been available to guide and test model development.

2. Experiments

[7] Our experiments took place in November 2005 at a location 55 miles due west of Moss Landing, CA. We contained and delivered the liquid CO_2 as described by *Peltzer et al.* [2004], using the MBARI ROV Tiburon for experimental control and data acquisition with the ROV mounted Simrad 1000 675 kHz sonar. The ROV was positioned directly under the ship's hull for data acquisition with the downward looking Simrad EK 500 38 kHz sonar, which had a maximum signal acquisition depth of about 1,000 m. Liquid CO_2 was dispensed into an acrylic "detritus sampler" of about 7.5 liter volume, 15 cm diameter, with an open bottom for introduction of the buoyant fluid, and a closed lid that could be opened under hydraulic control (Figure 1). Care was taken to minimize hydrate formation by turbulent mixing during the CO_2 loading step. The rapid opening of the sampler lid allowed the CO_2 to escape (1,000 m depth, 3.9°C, 34.370 salinity) with minimal resistance. The fluid began at once to break up due to Taylor instabilities (Figure 1), and no attempt was made to control droplet size.

[8] The rapidly rising, divergent, transparent fluid cloud is impossible to track visually and invasion of the cloud by the vehicle disturbs the signal. Larger globules of liquid rise faster than small droplets giving the cloud a changing and unknown vertical ascent characteristic; and the cloud is undergoing horizontal forcing from ocean currents as it rises. The dissolution rate is slow enough [*Brewer et al.*, 2002] that over the cloud lifetime it may experience quite varied physical forcing, and changing temperature, salinity, and thus density conditions. It is commonly assumed that pH sensing may be used to track a CO_2 plume, but for small releases the signal is undetectable, and slow dissolution and hydration kinetics [*Zeebe and Wolf-Gladrow*, 2001] greatly exacerbate the problem and thus some remote sensing technique is called for. In a small-scale pilot experiment carried out in late 2004 with the ROV Ventana we first recognized the remarkably sensitive acoustic detection of liquid CO_2 droplets but were unable at that time to track the cloud and constrain the experiment.

[9] The adopted strategy for tracking our moving invisible target was first to back-up the vehicle so that the rising cloud was several meters in front as detected by the scanning 675 kHz ROV sonar with a ±15° vertical cone. The ROV was then positioned about 10 m away from the cloud (Figure 2, top) and held stationary, thus giving the changing horizontal dimensions. Once the sonar signal indicated that the cloud had risen beyond view the ROV was piloted upwards, and positioned immediately above the cloud (the point at which no sonar signal was detected) and held stationary as the cloud moved up and out of view again. This yielded rise rate, and what are essentially a series of horizontal slices through the vertically moving cloud.

[10] At a depth of 1000 m both the CO_2 cloud, and the echo of the ROV, were detectable by the downward looking 38 kHz shipboard sonar (Figure 3a). This provided confirmatory response of the relative cloud-ROV positions, and also gave an indication of the cloud vertical extent at all

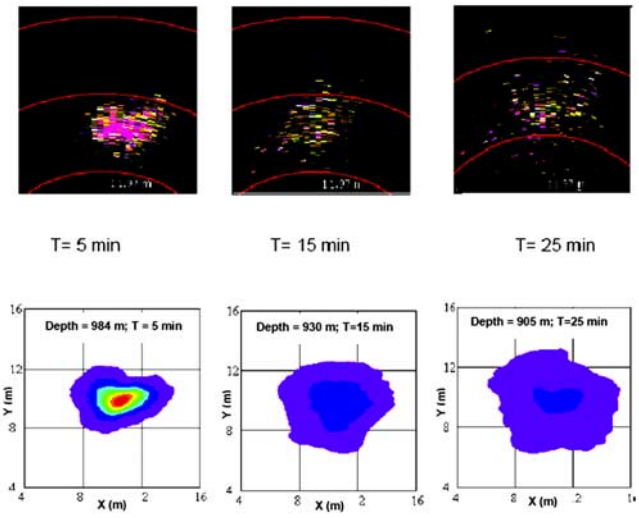

Figure 2. Comparison of the ROV borne 675 kHz sonar signal of horizontal slices through the rising cloud at 5, 15, and 25 minutes after release with a (top) numerical model [*Chen et al.*, 2003] and (bottom) with grid scales in meters.

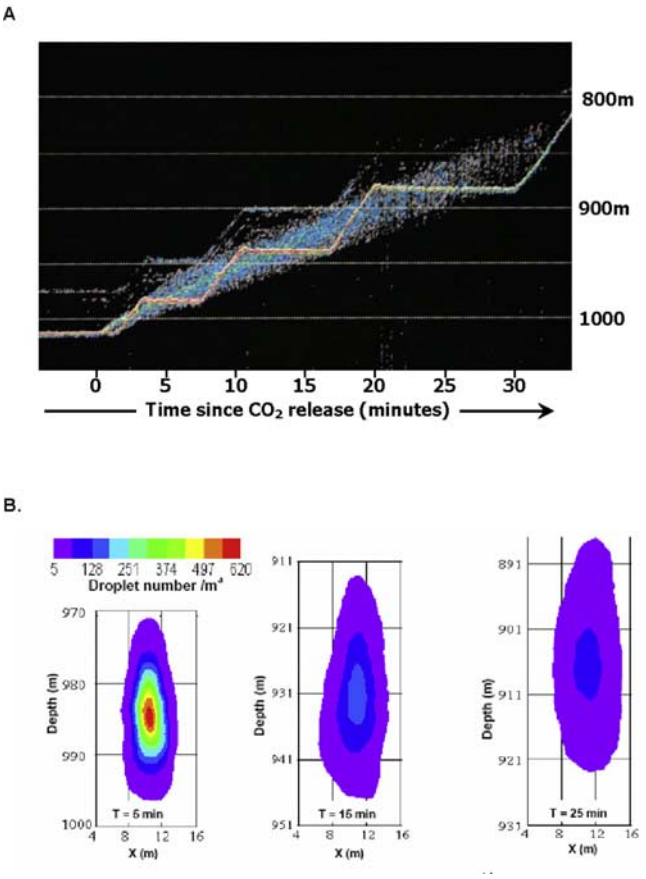

Figure 3. (a) Time series sonar image obtained from the downward looking Simrad EK 500 38 kHz system. The initial cloud release is at 1,000 m depth. The sharp, linear "stair case" return is from the ROV itself, the diffuse cloud is the return from the ascending CO_2 droplets. The vehicle itself is near-stationary in the horizontal, and the image is akin to a chart recording of the experiment. The observing strategy was to immediately back the vehicle away from the point of release so as to avoid disturbance of the cloud, and maintain 10–20 m horizontal separation. The vehicle was then flown above the cloud and then kept stationary while the cloud passed by; the sequence was then repeated. The cloud was detectable from the surface ship for over 30 minutes, and through 150 m of ascent. (b) Numerical model of the vertical extent of the cloud [*Chen et al.*, 2003] at 5, 15, and 25 minutes after release.

times. By combining both sonar data sets a three-dimensional picture in real time was obtained.

3. Results

[11] We were able to track the droplet cloud from the 1000 m CO_2 release for over 30 minutes and over 150 m of ascent (Figure 3a), giving an average ensemble rise rate for the cloud of about 5 m/min. This may be compared with the rise rate of from 6–9 m/min for the individual droplets measured by *Brewer et al.* [2002] using an imaging box technique and visual tracking. The difference is attributable to the different environmental conditions, release depths, and thus CO_2 physical properties. In the *Brewer et al.* [2002] study the release point was 804 m depth (T = 4.398°C, ρCO_2 = 0.9423 g/cc) and observation was lost at 341 m depth (T = 7.291°C, ρCO_2 = 0.8632 g/cc); the greater depth, and thus ocean and liquid CO_2 densities account for the slower rise rate. Changes in external water CO_2 chemistry between the two experiments are not significant in controlling the result.

4. Discussion

4.1. Comparison With Laboratory Studies

[12] The behavior of the droplets formed from the 5-L release has similarities to that observed for individual droplets studied in the laboratory under similar conditions in a high pressure tunnel [*Haljasmaa et al.*, 2005]. In the water tunnel experiments droplets much larger than 10 mm diameter were observed to shed CO_2 until approximately this diameter was reached, and rise rates of about 0.13 m/s were observed. Formation of a hydrate shell was not observed in the water tunnel experiments, whereas this is ubiquitous in natural sea water. Based upon the water tunnel experiments a dissolution rate of 3.5 μmol/cm^2/s is predicted at 1000-m depth and 4.1°C.

4.2. Comparison With Numerical Models

[13] We performed two numerical simulations of the 5-L release, one by a single CO_2 droplet simulation incorporating dissolution rates and buoyancy forces calibrated by laboratory and field studies to determine the initial sizes of droplets, and another by a turbulent two-phase cloud model [*Chen et al.*, 2003] to predict droplet cloud dynamics.

[14] The early single droplet observations [*Brewer et al.*, 2002] were described by a very simple spherical buoyancy equation applicable for a drag coefficient of 1:

$$u = 8gr(\rho_{sw} - \rho_{CO2})/3\rho_{CO2} \quad (1)$$

Where u is the terminal rise velocity, g is gravity, r is the droplet radius, and ρ_{sw} and ρ_{CO2} are the changing in situ densities of seawater and liquid CO_2 respectively. This approach was criticized [*Zhang*, 2005], but strongly supported in a rebuttal by *Alendal et al.* [2006]. The droplet sub-model used here for the slip velocity (u) and diameter-shrinking rate ($\dot{d}$) is of the form:

$$\dot{u}_c = \frac{\rho_s}{\rho_c}\left[\left(1 - \frac{\rho_c}{\rho_s}\right)g - \frac{3u_c^2}{4d_c}C_d\right] - u_c\frac{\dot{m}_c}{m_c} \quad (2)$$

$$\dot{d}_c = -\frac{1}{\rho_c}\left(\frac{d_c}{3}\dot{\rho}_c + \frac{2Sh_eD_f(C_{cs} - C_s)}{d_c}\right) \quad (3)$$

Where m, ρ, and C are the mass of the droplet, the density, and the CO_2 concentration respectively. The subscripts c, cs, and s indicate CO_2, CO_2 droplet surface, and seawater respectively. Sh_e and C_d are the effective Sherwood number and effective drag coefficient respectively. The dotted symbols are derivatives with respect to time. The last two parameters play a key role in the prediction of droplet dissolution and rising velocity. Here the experimental data based values of Sh_e and C_d given by *Chen et al.* [2003] are used in the simulations.

[15] Field and laboratory observations, and model predictions, show that the droplets formed rapidly after free liquid release range from 8 to 10 mm diameter. Over the observed CO_2 cloud ascent from the release depth of 1,000 m to 850 m (4.8°C) we calculate from the droplet sub-model that a droplet with an initial diameter of 10 mm will decrease in size to 4.7 mm, and the rise velocity will decrease from 0.11 m/s to 0.08 m/s. A droplet with an initial 8 mm diameter will decrease to 1 mm, and the velocity decrease is from 0.10 m/s to 0.02 m/s.

[16] We use droplet number density (number/m^3) to visualize the CO_2 cloud dynamics from the two-phase modeling simulations. With initial diameters of 8–10 mm set randomly droplets disperse horizontally due to local water velocities, while rising vertically (Figure 3b). Our simulations of vertical sections are well matched to the sonar images for up to 15 minutes from release not only for the height of the CO_2 cloud but also for cloud width. The simulated cloud rises slowly with a slightly lower velocity in comparison with that detected by sonar at 25 minutes. This may be due to a downward flow predicted in the model by locally dense CO_2 enriched sea water [*Chen et al.*, 2005]. Because of a relatively smaller computation domain in the horizontal (20 m × 20 m) than the vertical (200 m), the open boundary conditions at top and bottom make the modeled flow field sensitive to the small negative buoyancy effect. This predicted downward flow developed to a detectable level in comparison with the droplet rise velocities after about 20 minutes, when CO_2 dissolution caused the small droplets to rise with lower velocity. In the real ocean no significant down-welling was observed, since the small size of the release produced negligible local density increases. We note that in earlier published work [*Brewer et al.*, 2002] a small programming error in the simple model used lead to a slight exaggeration of rise rate for small droplets late in the plume development.

[17] For modeled horizontal sections simulations agreed well with the ROV sonar record with modeled and observed scales of 12 × 12 m^2 in cloud/droplet areas. The cloud dilutions detected by the ROV sonar correspond to simulations with maximum droplet number densities of 620, 160, and 80 at each sampled time (5, 15, and 25 minutes) respectively.

5. Conclusions

[18] While direct comparisons with acoustic detection of the more commonly observed methane gas bubble clouds [*Heeschen et al.*, 2003] are difficult, there is every indication of extraordinarily sensitive acoustic detection for a liquid CO_2 release within the hydrate formation zone, and we may ask why this should be so. Although methane gas clouds form a hydrate skin, observations [*Rehder et al.*, 2002] suggest that the tensile strength of the film is not sufficient to completely overcome the distortion of the rising bubble shape due to buoyancy forces. The greater density and thus lower rise rate of liquid CO_2 droplets reduces the buoyancy, and the tensile strength of the hydrate film, ≅0.1 N/m under these conditions [*Yamane et al.*, 2000], is sufficient to overcome distortions and produce a near perfect spherical shape of high velocity contrast, creating a highly efficient acoustic scatterer. There is excellent agreement between models and field work, suggesting that quite accurate predictions can be made of the fate of CO_2 clouds in the deep ocean. The results suggest that very sensitive detection of small amounts of liquid CO_2 leaking from the sea floor may be detected acoustically, but that rapid dissolution of the cloud results in signal detection only within about 150 m of vertical ascent from the source. The experiment reported here was of small enough scale that no significant seawater density changes resulted from CO_2 dissolution, and at the frequencies used here acoustic detection of the dissolved CO_2 is not possible. However even quite subtle density changes in sea water may be detected at lower frequencies [*Holbrook et al.*, 2003], and thus for larger releases detection of the near-field dissolved plume may be achievable. Since the use of acoustics for biological detection is well established, this tool also offers a unique way to detect water column biological responses to liquid CO_2 released from the sea floor. We were not able to measure directly the change in pH field resulting from such a small release, and that remains a challenge for future work.

[19] **Acknowledgments.** We thank the pilots of the ROV Tiburon, and captain and crew of the R/V *Western Flyer* for expert help at sea. The work was supported by grants from the David and Lucile Packard Foundation (MBARI), and the U.S. Department of Energy. Baixin Chen was financially supported through the ARCS project, NETO, Japan.

References

Alendal, G., and H. Drange (2001), Two-phase, near-field modeling of purposefully released CO_2 in the ocean, *J. Geophys. Res.*, *106*, 1085–1096.

Alendal, G., P. M. Haugan, R. Gangsto, K. Caldeira, E. Adams, P. G. Brewer, E. T. Peltzer, G. Rehder, T. Sato, and B. Chen (2006), Comment on "Fate of Rising CO_2 Droplets in Seawater" by Y. Zhang, *Environ. Sci. Technol.*, *40*, 3653–3654.

Barry, J. P., K. R. Buck, C. F. Lovera, L. Kuhnz, P. J. Whaling, E. T. Peltzer, P. Walz, and P. G. Brewer (2004), Effects of direct ocean CO_2 injection on deep-sea meiofauna, *J. Oceanogr.*, *60*, 759–766.

Brewer, P. G. (1997), Ocean chemistry of the fossil fuel CO_2 signal: The haline signature of "business as usual", *Geophys. Res. Lett.*, *24*, 1367–1369.

Brewer, P. G., G. Friederich, E. T. Peltzer, and F. M. Orr Jr. (1999), Direct experiments on the ocean disposal of fossil fuel CO_2, *Science*, *284*, 943–945.

Brewer, P. G., E. T. Peltzer, G. Friederich, and G. Rehder (2002), Experimental determination of the fate of rising CO2 droplets in sea water, *Environ. Sci. Technol.*, *36*, 5441–5446.

Caldeira, K., and M. E. Wickett (2003), Anthropogenic carbon and ocean pH, *Nature*, *425*, 365.

Callendar, G. S. (1938), The artificial production of carbon dioxide and its influence on temperature, *Q. J. R. Meteorol. Soc.*, *64*, 223–240.

Chen, B., Y. Song, M. Nishio, and M. Akai (2003), Large-eddy simulation of double cloud formation induced by CO_2 dissolution in the ocean, *Tellus, Ser. B*, *55*, 723–730.

Chen, B., Y. Song, M. Nishio, S. Someya, and M. Akai (2005), Modeling near-field dispersion from direct injection of carbon dioxide into the ocean, *J. Geophys. Res.*, *110*, C09S15, doi:10.1029/2004JC002567.

Cicerone, R., J. Orr, P. G. Brewer, P. Haugan, L. Merlivat, T. Ohsumi, S. Pantoja, and H. O. Poertner (2004), The ocean in a high CO_2 world, *Eos Trans. AGU*, *85*, 351, 353.

DeLucia, E. H., J. G. Hamilton, S. L. Naidu, R. B. Thomas, J. A. Andrews, A. Finzi, M. Lavine, R. Matamala, J. E. Mohan, G. R. Hendrey, and W. H. Schlesinger (1999), Net primary production of a forest ecosystem with experimental CO_2 enrichment, *Science*, *284*, 1177–1179.

Figueiredo, M. A., D. M. Reiner, and H. J. Herzog (2003), Ocean carbon sequestration: A case study in public and institutional perceptions, in *Greenhouse Gas Control Technologies: Proceedings of the 6th International Conference on Greenhouse Gas Control Technologies, 1–4 October 2002, Kyoto, Japan*, 1st ed., edited by J. Gale and Y. Kaya, pp. 799–804, Elsevier, New York.

Gangstø, R., P. M. Haugan, and G. Alendal (2005), Parameterization of drag and dissolution of rising CO_2 drops in seawater, *Geophys. Res. Lett.*, *32*, L10612, doi:10.1029/2005GL022637.

Haljasmaa, I. V., J. S. Vipperman, R. J. Lynn, and R. P. Warzinski (2005), Control of a fluid particle under simulated deep-ocean conditions in a high-pressure water tunnel, *Rev. Sci. Instrum.*, *76*, 025111.1–025111.11.

Heeschen, K. U., A. M. Tréhu, R. W. Collier, E. Suess, and G. Rehder (2003), Distribution and height of methane bubble plumes on the Cascadia Margin characterized by acoustic imaging, *Geophys. Res. Lett.*, *30*(12), 1643, doi:10.1029/2003GL016974.

Holbrook, W. S., P. Paramo, S. Pearse, and R. W. Schmitt (2003), Thermohaline fine structure in an oceanographic front from seismic reflection profiling, *Science*, *301*, 821–824.

Intergovernmental Panel on Climate Change (IPCC) (2005), *Special Report on Carbon Dioxide Capture and Storage*, edited by B. Metz et al., 431 pp., Cambridge Univ. Press, Cambridge, New York.

Lupton, J., et al. (2006), Submarine venting of liquid carbon dioxide on a Mariana Arc volcano, *Geochem. Geophys. Geosyst.*, *7*, Q08007, doi:10.1029/2005GC001152.

Peltzer, E. T., et al. (2004), Initial results from a 4 km CO2 release experiment, *Preprints Pap. Presented Am. Chem. Soc. Div. Fuel Chem.*, *49*, 429–430.

Portner, H. O., M. Langenbruch, and A. Reipschlager (2004), Biological impact of elevated ocean CO_2 concentrations: Lessons from animal physiology and earth history?, *J. Oceanogr.*, *60*, 705–718.

Rehder, G., P. W. Brewer, E. T. Peltzer, and G. Friederich (2002), Enhanced lifetime of methane bubble streams within the deep ocean, *Geophys. Res. Lett.*, *29*(15), 1731, doi:10.1029/2001GL013966.

Royal Society (2005), Ocean acidification due to increasing atmospheric carbon dioxide, report, 60 pp., Clyvedon Press, Cardiff, UK.

Sabine, C. L., et al. (2004), The oceanic sink for anthropogenic CO_2, *Science*, *305*, 367–371.

Sakai, H., T. Gamo, E.-S. Kim, M. Tsutsumi, T. Tanaka, J. Ishibashi, H.Wakita, M. Yamano, and T. Oomori (1990), Venting of carbon dioxide-rich fluid and hydrate formation in mid-Okinawa Trough back arc basin, *Science*, *248*, 1093–1096.

Sato, T. (2004), Numerical simulation of biological impact caused by direct injection of carbon dioxide in the ocean, *J. Oceanogr.*, *60*, 807–816.

Seibel, B. A., and P. J. Walsh (2001), Potential impacts of CO_2 injection on deep-sea biota, *Science*, *294*, 319–320.

Wigley, T. M. L., R. Richels, and J. A. Edmonds (1996), Economic and environmental choices in the stabilization of atmospheric CO_2 concentrations, *Nature*, *379*, 240–243.

Yamane, K., I. Aya, S. Namie, and H. Nariai (2000), Strength of CO_2 hydrate membrane in sea water at 40 MPa, *Ann. N. Y. Acad. Sci.*, *912*, 254–260.

Zeebe, R. E., and D. A. Wolf-Gladrow (2001), *CO_2 in Seawater: Equilibrium, Kinetics, Isotopes*, 345 pp., Elsevier, New York.

Zhang, Y. (2005), Fate of rising CO_2 droplets in seawater, *Environ. Sci. Technol.*, *39*, 7719–7724.

A. Baggeroer, Department of Ocean and Electrical Engineering, Massachusetts Institute of Technology, Room 5-204, Cambridge, MA 02139, USA.

P. G. Brewer, R. M. Dunk, E. T. Peltzer, and P. Walz, Monterey Bay Aquarium Research Institute, 7700 Sandholdt Road, Moss Landing, CA 95039, USA. (brpe@mbari.org)

B. Chen, National Institute of Advanced Industrial Science and Technology, 1-2-1 Namiki, Tsukuba 305-86564, Japan.

R. Warzinki, National Energy Technology Laboratory, U.S. Department of Energy, P.O. Box 10940, Pittsburgh, PA 15236, USA.

Scaled-up Ocean Injection of CO_2-Hydrate Composite Particles

C. Tsouris*, P. Szymcek, P. Taboada-Serrano, S. McCallum
Oak Ridge National Laboratory

P. Brewer*, E. Peltzer, P. Walz
Monterey Bay Aquarium Research Institute

E. Adams*, A. Chow
Massachusetts Institute of Technology

K. Johnson
Institute of Ocean Sciences of Canada

J. Summers
U.S. Department of Energy

Prepared for publication in

Environmental Science and Technology

October 2006

*Corresponding authors:
Costas Tsouris, tsourisc@ornl.gov, 865-241-3246 (reactor scaleup and laboratory experiments)
Peter Brewer, brpe@mbari.org, 831-775-1706 (field experiments)
Eric Adams, eeadams@MIT.EDU, 617-253-6595 (plume simulations)

Scaled-up Ocean Injection of CO_2-Hydrate Composite Particles

C. Tsouris*, P. Szymcek, P. Taboada-Serrano, S. McCallum
Oak Ridge National Laboratory

P. Brewer*, E. Peltzer, P. Walz
Monterey Bay Aquarium Research Institute

E. Adams*, A. Chow
Massachusetts Institute of Technology

K. Johnson
Institute of Ocean Sciences of Canada

J. Summers
U.S. Department of Energy

Abstract

A pilot-scale, three-phase, continuous-jet hydrate reactor, developed to produce carbon dioxide hydrate for ocean sequestration, was tested both in the laboratory and at sea. A 72-L pressure vessel was used for laboratory tests; field experiments were performed with a remotely operated vehicle at depths between 1200 and 2000 m in Monterey Bay, California. Rapid production of consolidated, sinking CO_2-hydrate composite particles was achieved in both settings. The vertical and lateral movement of particles in the ocean was monitored by the vehicle high-definition television camera and with a 675-kHz sonar, along with dissolution rates and associated T and pH changes during the injection operations. It was observed that globules of unconverted liquid CO_2 occluded in the structure of the hydrate aggregates largely determine their behavior in the ocean by providing sites for accelerated dissolution, thereby affecting aggregate shape, lifetime, and sinking rate.

K**eywords:** Gas hydrate reactor, carbon dioxide hydrate, ocean carbon sequestration

*Corresponding authors:
Costas Tsouris, tsourisc@ornl.gov, 865-241-3246 (reactor scaleup and laboratory experiments)
Peter Brewer, brpe@mbari.org, 831-775-1706 (field experiments)
Eric Adams, eeadams@MIT.EDU, 617-253-6595 (plume simulations)

Introduction

Global atmospheric emissions of CO_2 are predicted to increase from 7.4 Gt carbon (GtC) per year in 1997 to 26 GtC per year by 2100 (*1*). Ocean sequestration of CO_2 is a possible method to counteract the increase in atmospheric CO_2. Estimates show that up to 300 GtC can be stored in the deep ocean without increasing the pH by more than 0.18 units, which is comparable to levels of observed natural variability (*2*). Proposed methods for marine sequestration include liquid CO_2 injection at intermediate depths to produce a rising and gradually dissolving plume of CO_2 droplets, sequestration of solid CO_2-hydrate to produce a plume of sinking, gradually dissolving particles, and injection of sinking liquid CO_2 at depths larger than 3000 m to form a liquid-CO_2 lake in the bottom of the ocean.

Several aspects have to be taken into consideration when deciding on an ocean sequestration alternative. The first aspect deals with the environmental impacts of the selected injection method. Injection of liquid CO_2 and injection of CO_2-hydrate particles are expected to cause lesser environmental effects because of the dispersed, slowly dissolving plumes produced in both methods. In addition, solid CO_2-hydrate particles sink to greater depths after formation (*3*,*4*), or to zones of pressure and temperature of increased hydrate-phase thermodynamic stability (*5*,*6*). Therefore, sinking hydrate particles present the additional advantage of slower dissolution rates and less impact to shallow-depth, life-rich marine environments. The second aspect to be taken into consideration is the operational costs involved in the injection process. Infrastructure and implementation costs of most injection methods increase with injection depth, while residence times for sequestered CO_2 increase with increasing depth (*7*). Although injection costs for CO_2-

hydrate sequestration may be slightly higher than those for liquid CO_2 injection at the same depth, CO_2-hydrate sequestration constitutes a reasonable compromise between injection costs and environmental impacts.

A laboratory-scale continuous-jet hydrate reactor (CJHR) was developed at Oak Ridge National Laboratory (ORNL) to produce hydrate (*3,8*). This reactor was initially designed to produce CO_2 hydrate for marine carbon dioxide sequestration (*8*), and was also tested in the field to verify its effectiveness (*4,9*). The laboratory-scale CJHR was able to achieve conversions of up to 30 % in a laboratory setting (*3,8*) and conversions of 45 % during field-testing operations (*4,9*). Since conversions larger than 20 % result in effective injections (i.e., sinking, cohesive CO_2-hydrate particles) at injection depths larger than 1200 m, the laboratory version of the CJHR was quite successful. However, if the goal to capture approximately 175 GtC over a period of 50 years is to be achieved (*10*), intensive and large capacity CO_2-hydrate injectors will be required.

The field testing of a pilot-scale CJHR is described in this work. The original laboratory-scale reactor design (*3,4,8,9*) was modified to allow for at least a ten-fold increase in volumetric flow, while maintaining high conversions. Different injector designs were initially tested in the laboratory for the reactor presented in Figure 1(a), and the more promising ones were chosen for the field experiments detailed in this work. For the field experiments, a battery of four CJHRs in series was designed to further increase CO_2-hydrate production capacity, and to obtain data on the fate of the CO_2-hydrate particles produced. Information from field experiments was introduced into a plume-modeling scheme to generate possible outcomes of large-scale, CO_2-hydrate injection operations. The modeling results are an important contribution towards the

assessment of the behavior of the plume, residence time of CO_2 in the ocean, and ultimately environmental impacts of CO_2 ocean sequestration as gas hydrate.

The Continuous Jet Hydrate Reactor

The CJHR used in this study constitutes a scaled-up version of the original reactor developed at Oak Ridge National Laboratory (*3,4,8,9*). The laboratory-scale reactor was designed to produce sinking and cohesive CO_2 hydrate particles to ensure successful ocean carbon sequestration. The particles produced by the CJHR were heterogeneous, cohesive aggregates composed of CO_2-hydrate particles and unconverted liquid CO_2. The characteristics of the hydrate particles produced had to be maintained during the scale-up process.

The density of the hydrate particles relies heavily upon the conversion of CO_2 into hydrate. The particles will sink when approximately 25% of the injected CO_2 is converted into hydrate at depths greater than 1000 meters. The formation of CO_2 hydrate constitutes a product-limited reaction (*11*). Hydrate formation occurs instantaneously when H_2O and liquid CO_2 interact at given temperatures and pressures. This reaction forms a solid layer of CO_2 hydrate at the interface of the two species. Essentially, the solid hydrate limits further formation of hydrate, and hence this process is controlled by mass transfer through the surface area along which the two species interact. Therefore, the potential of hydrate formation is limited by a surface barrier to mass transfer that prevents the interaction between the two reactants. In addition to mass transfer effects, thermal effects are important during hydrate formation. Hydrate formation constitutes an exothermic reaction (*6*). Considerable localized temperature increase may occur

upon reaction at the interface between reactants, if heat is not effectively dissipated by the system. Significant increase in temperature may hinder further hydrate formation because the system could move away from the thermodynamically favorable conditions for hydrate formation (i.e., conditions of pressure and temperature inside the hydrate-phase stability zone). The combination of mass transfer barriers with slow dissipation of reaction heat decreases the final conversion achieved during hydrate production.

Mass transfer barriers can be reduced via increasing surface area of interaction between reactants. Larger interfacial areas also increase heat transfer from the interface into the bulk of the reactants, where the excess heat generated by the reaction can be absorbed. Therefore, the pilot-scale CJHR had to be designed to increase surface area (i.e., increase the amount of H_2O and CO_2 converted into hydrate), while working with larger flowrates of reactants—approximately a ten-fold increase in production capacity.

Maximizing surface area can be achieved by dispersing one of the hydrate-forming species into the continuous flow of the other hydrate forming species (i.e., dispersing CO_2 in H_2O or vice versa). Ideally, the dispersed phase should be sprayed into the continuous phase with the smallest droplet size possible. It is desirable for the dispersion of one reactant into the other to be performed under spray mode conditions (*12*). At these hydrodynamic conditions, the dispersed phase will be present in very fine droplets, increasing interfacial area, reducing mass-transfer barriers for the reaction, and maintaining large conversions even at high flowrates.

The pilot-sale CJHR is a tubular reactor that consists of a 13.3-cm headpiece with interchangeable inputs for gas and H_2O, and a 45.7-cm long Teflon tube that acts as the mixing zone. The dispersed phase species flows through a single inlet on the top of the headpiece into an exchangeable injector of 1.27-cm length and varying designs (Figure 1a). The reactant that constitutes the continuous phase flows into the reactor through an inlet directly below the exchangeable injector piece. The two phases mix below the injector to form hydrate, which becomes consolidated in the mixing zone due to hydrate forming at the boundaries of the droplets (Figure 1b). The reactor design allows for the testing of different injection modes and different choices of dispersed phase to be tested. Capillaries embedded in the injector (head piece disc) were chosen to distribute the flow of the dispersed reactant into the continuous one. Capillary sizes and configurations were tested in terms of their ability to produce a spray jet break-up regime at high flowrates and low back-pressures. The injector design chosen includes an array of capillaries, six of them in the periphery and one in the center of the distributing disc. The smaller diameters of multiple capillaries with similar total cross sectional area to that of a single-capillary injector (i.e., the original design of the laboratory-scale injector) allow for a spray-mode jet break-up regime while sustaining a high flowrate.

Experimental Methods

During the preliminary laboratory tests, the CJHR was mounted inside the Seafloor Process Simulator (SPS), which is used to simulate CO_2-hydrate injection in marine environments (*13*). The SPS is a cylindrical Hastelloy C-22 vessel of diameter 31.75 cm, length = 91.44 cm, and volume = 72 L (*13*). The vessel is equipped with several sapphire windows and sampling ports,

and can be maintained at a pressure of up to 20 MPa. The SPS allows operation pressures equivalent to different ocean depths to be maintained during laboratory experiments. The entire reactor was submerged and at equilibrium with the vessel. A Seabird SBE ST pump (Seabird Electronics, Bellevue WA) was used to circulate H_2O within the SPS at a controlled flowrate into the CJHR where it was mixed with liquid CO_2 injected from outside the SPS by a Haskel ALG-15/30 pulsed-flow pump (Haskel, Burbank CA). The laboratory tests reported in this work were performed with flowrates between 2.00 and 3.00 L/min H_2O, and 0.40 and 0.66 L/min CO_2. The recirculation of H_2O and the external introduction of CO_2 simulated injection operations in the field. Experiments were conducted with both distilled and simulated ocean H_2O. The salinity of simulated ocean H_2O was kept at 35 ppt using Instant Ocean® (Aquarium Systems, Mentor OH). The SPS was configured with a pressure transducer and thermocouples monitoring pressure and H_2O and headspace temperatures within the SPS. LabView software was used to monitor and record internal pressure and temperature conditions. The SPS was filled with approximately 60 L of distilled or saline H_2O, and nitrogen was used to pressurize the vessel. Gas was periodically vented from the SPS during experiments to maintain the pressure at a preset value. This approach caused the pressure to vary within a range of 0.50 MPa during experiments. The experiments were visually recorded with a Sony Firewire (XCD-X710CR) camera connected to a personal computer.

Field experiments were conducted using a battery of four CJHRs mounted in series, identical to the one used in laboratory experiments (Figure 1c). The CJHR was mounted on the remotely operated vehicle (ROV) *Tiburon*. Experiments were monitored aboard the research vessel (RV) *Western Flyer* near the coast of Monterey Bay, CA. A _____ pump was used to

circulate ocean H_2O into the CJHRs. CO_2 flow was regulated by draining pressure from a pressurized CO_2-reservoir. Two injector designs with multiple capillaries of diameters equal to 0.794 and 1.191 mm were selected for the field experiments based on their ability to produce consolidated, sinking hydrate particles at pressures as low as the ones equivalent to depths of 1000 m. The injectors could also work with high flowrates while maintaining low back pressures and not producing clogging problems. Experiments were conducted with either H_2O or liquid CO_2 as the dispersed phase. H_2O flowrates ranged from 3.50 L/min to 8.00 L/min, and liquid CO_2 flowrates ranged from 1.50 L/min to 3.00 L/min. Experiments were conducted at depths ranging from 1200 to 2000 meters below the surface. Salinity and temperature changed depending upon ambient ocean conditions, and were monitored using _____installed on the ROV *Tiburon*. Field experiments focused on monitoring the fate of individual hydrate particles. After the formation of hydrate composites, a single particle was arbitrarily selected, and its vertical movement was monitored by the primary high-definition television (HDTV) camera system installed on the ROV *Tiburon* (*14*). The selected particle was followed until it became visually indistinguishable. At this point, it was assumed that the particle had nearly dissociated. The lateral movement of all the produced particles (i.e., the development of a plume) was monitored by a 675-kHz sonar system installed on the RV *Western Flyer*. The pH of the surrounding water was monitored by two pH probes, model 18-I (Seabird Electronics, Bellevue WA), installed on the ROV *Tiburon*.

Results and Discussion

Jet-break up regimes for laboratory and field experiments

Laboratory tests of the pilot-scale CJHR were conducted in order to choose injector designs suitable for the field experiments. These tests were also performed to determine optimum operating conditions for the CJHR. (Temperature and pressure conditions were selected to reflect those of ambient temperatures of the intermediate depths of Monterey Bay, CA.) Dispersed phases (CO_2 or H_2O), flowrates, and capillary sizes and configurations were selected to yield spray-mode flow regimes. Spray-mode conditions prevail for Weber numbers (We) greater than 324 during dispersion of liquid CO_2 in H_2O and vice versa (*12*). However, during hydrate formation, better results are obtained for We numbers equal or greater than 1024.

The first part of Table 1 summarizes the results obtained in terms of jet break-up regimes for the two multiple-capillary injectors chosen for the field experiments. The laboratory experiments listed in Table 1, which correspond to field conditions, resulted in jet-break up regimes in spray-mode (We > 324) in all cases. Furthermore, all but one laboratory experiment achieved We > 1024. The utilization of CO_2 as dispersed phase resulted in jet-break up regimes in spray-mode with high associated We numbers (We = 7454 and We = 25158 for the two H_2O:CO_2 ratios examined, respectively). The utilization of H_2O as dispersed phase on the other hand, resulted in lower We numbers (between We = 1017 and We = 7725, for the two injectors selected and different H_2O:CO_2 ratios).

Figure 2 presents temperature profiles (i.e., temperature in different parts of the CJHR vs. injection time) for laboratory experiments at conditions of experiments Lab-1 to Lab-4, listed in Table 1. Although the bulk temperature and the temperature at the injector itself (exchangeable head-piece) remain close to the base-line ambient temperature, the temperature in the mixing zone and at the outlet of the CJHR (outlet of Teflon tube) experience an increase of 4 to 6 °C, in some cases. The more marked temperature increase occurs in the mixing zone, where the reaction is led to near completion. Although the increase in temperature at higher pressures (e.g., P = 13.8 MPa) does not drive the system to thermodynamically unfavorable conditions for hydrate formation, as pressure diminishes or at shallower injection depths, the same increase in temperature may have detrimental effects on hydrate formation. One should note that the magnitude of temperature increase during reaction is not affected by pressure, and that this increase can be controlled by the degree of dispersion or We number achieved during operation of the reactor.

The reduction of mass transfer barriers and thermal effects achieved with better dispersion of one reactant into the other (i.e., higher We numbers) could be directly observed on the characteristics of the hydrate product in terms of degree of consolidation and buoyancy. In general, during laboratory experiments, the utilization of CO_2 as dispersed phase yielded sinking CO_2-hydrate particles at all the conditions reported above, with the degree of consolidation increasing with increasing We number. Experiments with H_2O did also produce sinking hydrate particles, but the degree of consolidation was less than that of the particles obtained with CO_2 dispersed, which corresponds to the lower We numbers achieved at these conditions. Additionally, smaller capillary sizes resulted in more consolidated hydrates. Based on the analysis of laboratory

results, the 1.191-mm multiple-capillary injector was selected for experiments in the field using CO_2 as the dispersed phase, and the 0.794-mm multiple-capillary injector was selected for experiments in the field with H_2O as the dispersed phase. Additionally, a minimum value of 2.5 for the H_2O:CO_2 ratio was recommended for the field experiments at P = 11.8 MPa (equivalent to an approximate depth of 1200 m).

The second part of Table 1 displays the jet break up regimes observed during field experiments in terms of values of the We number. Higher We numbers were obtained when H_2O was used as dispersed phase than when CO_2 was used as dispersed phase during field experiments. We numbers between 10514 and 54930 were obtained in the field when H_2O was used as the dispersed phase. This behavior was expected because higher H_2O flowrates were used in the field than in the laboratory for comparable capillary diameters. On the other hand, when CO_2 constituted the dispersed phase, We numbers between 1540 to 2218 were obtained, despite the fact that higher flowrates of CO_2 were used in the field than during laboratory experiments for comparable capillary diameters. A possible explanation for this behavior lies on the fact that a pulsed-flow pump was used for CO_2 during laboratory experiments, while in field experiments, both pumps were continuous. The calculated CO_2 flow during individual pulses was equivalent to 5.5 L/min of CO_2, which leads to We numbers of 7454 and 25148 for the 1.191-mm and 0.794-mm multiple-capillary injectors, respectively. It should also be noted that the reason for laboratory experiments to be conducted with a pulsed-flow pump providing a lower maximum flowrate than the flowrate achieved by a steady-flow pump in the field is because of limitations in total throughput in the SPS.

Since the jet break up regime achieved during injection operations is directly related to the characteristics of the hydrate product obtained, it was expected that more cohesive, sinking CO_2-hydrates would be obtained with H_2O as dispersed phase during field experiments. It was also expected that higher conversions would be obtained in this case as well, because higher We numbers or more pronounced spray-mode regimes would result in smaller mass transfer and thermal barriers for the hydrate formation reaction.

Vertical movement of CO_2-hydrate aggregates

The vertical movement of selected particles from each batch of experiments was visually recorded, and it is presented in this work as the vertical position of the particle vs. time after injection (i.e., depth vs. time profiles or vertical movement profiles). The particles dissolved as they moved downwards or upwards, and the recording was stopped as soon as the particles were no longer distinguishable. Experiments performed with different injections and using different species as the dispersed phase are listed with a code, e.g., TO967, which is related to the RV logging system. An additional number is used to identify different conditions of flowrate and injection depths within experiments performed with the same injector and the same dispersed phase.

Figure 3 presents the vertical movement profiles of CO_2-hydrate particles obtained using CO_2 as the dispersed phase and the 1.191-mm multiple-capillary injector. The selected CO_2-hydrate particle produced at an injection depth of 1750 m was initially neutrally buoyant, sinking to greater depths after 4 to 5 minutes. The CO_2-hydrate particles produced at injection depths of

2000 m did sink almost immediately, though a small period of neutrally buoyancy (less than 1 minute) was observed in both cases. The "lag" period or the time interval at which the recently produced particles were neutrally buoyant can be associated to the amount of unconverted liquid CO_2 trapped inside the aggregate in between individual hydrate particles. Although CO_2-hydrate is denser than ocean water by approximately 10 %, liquid CO_2 becomes denser than seawater only at depths larger than 3000 m. Therefore, the amount of unconverted, liquid CO_2 trapped inside the CO_2-hydrate aggregates makes them either buoyant or neutrally buoyant when the hydrate aggregates are just synthesized. However, the dissolution of liquid CO_2 is faster than that of solid hydrate, and therefore, the remaining solid hydrate-aggregate backbone sinks as it slowly dissolves, once enough liquid CO_2 trapped in the hydrate aggregates has been dissolved. The amount of unconverted liquid CO_2 does not only affect the relative density of the hydrate aggregates, but also their shape. More malleable aggregates result from higher amounts of occluded liquid CO_2 in the aggregate structure. These aggregates acquire long helicoidal shapes during injection operations. The shape of the aggregates affects their settling velocity, resulting in the non-continuous, sometimes non-linear vertical movement profiles observed in Figure 3. The aggregate may be propelled to greater depths, if shaped like an elongated cork screw, or it may even become neutrally buoyant if the helicoid is closely packed.

Figure 4 presents the vertical movement profiles of particles produced in experiments TO969, where seawater was used as dispersed phase at high H_2O:CO_2 ratios. Cohesive, sinking CO_2-hydrate aggregates were produced at lower injection depths than in the case of CO_2 as dispersed phase, which indicates a higher conversion. This conclusion is further sustained by two observations. First, the aggregates traveled longer vertical distances in comparable times to the

ones produced with CO_2 as dispersed phase. Second, the aggregates were brittle and broke into short cylinders upon formation, i.e., they contained less amount of unconverted liquid CO_2 occluded in their structures. The fact that these aggregates dissolved faster than the ones produced with CO_2 as dispersed phase is only a consequence of the thermodynamic conditions (pressure and temperature) associated to Figure 4 being less favorable towards hydrate stability than the conditions depicted in Figure 3. Although aggregates TO969-1 and TO969-2 were produced at identical conditions, and at the same injection depth, one of them presents larger average sinking velocities than the other. In fact, particle TO969-2 seems to present three different zones in terms of sinking velocities (i.e., different slopes of the depth vs. time profiles). In this case, the shape individual aggregates acquired as they dissolved (the aggregates did not seem to dissolve uniformly) determined their orientation in the liquid column, and ultimately the behavior of the vertical movement profiles.

Figure 5 presents the depth profiles for the CO_2-hydrate aggregates produced in experiments TO970, in which H_2O was also used as the dispersed phase, but with lower H_2O:CO_2 ratios. In this case, the hydrate aggregates were also brittle and cylindrical. The vertical movement profiles of particles TO970-4 and TO970-6 present an initial lag time due to occluded liquid CO_2 dissolution, as discussed earlier. On the other hand, aggregate TO970-3 sank immediately, hinting that the fraction of occluded unconverted CO_2 was not large enough to make the aggregate buoyant. As expected, the amount of unconverted liquid CO_2 increased as injection depth decreased due to the increasingly thermodynamically unfavorable conditions for hydrate formation found at shallower depths. As in previous cases, aggregates TO970-4 and TO970-6 sank readily after a critical amount of occluded CO_2 was dissolved. In the cases presented in

Figure 4, there is a slight non-linearity of the vertical movement profiles. The changes in settling velocity result from tumbling and reorientation of the aggregates within the vertical column of water, which greatly affect the drag coefficient. The preferential orientations of hydrate aggregates result from local differences in density within the aggregates, which originate from the initial non-uniform distribution of occluded CO_2 and from non-uniform dissolution rates of the solid hydrate particles. However, one should note that the vertical movement profiles of aggregates produced with H_2O as the dispersed phase present a more linear behavior than their peers produced with CO_2 as dispersed phase. The reason is because better mixing conditions in the CJHR reactor lead to higher conversion of liquid CO_2 to hydrate. The mixing conditions are in general better (e.g., higher We numbers), in this case, because of higher flow velocities of the jets through the capillaries of the distributor. On the other hand, for the laboratory experiments where a pulsed-flow pump was used for liquid CO_2 with CO_2 as the dispersed phase, results were better because of the lower viscosity of liquid CO_2, and because the jet velocity was kept high during each pulse.

In conclusion, the use of H_2O as dispersed phase allows for the formation of plumes of solid hydrate aggregates of more uniform shape, higher relative density, almost constant settling velocities, and slower dissolution rates. This responds to the fact that higher We numbers can be achieved with water as dispersed phase, diminishing detrimental mass-transfer and thermal effects. The fact that water has a high heat capacity and acts like a good heat sink may have constituted an additional advantage during field experiments with H_2O as the dispersed phase, besides the fact that the CJHRs were submerged in a large body of water.

Dispersion of CO_2-hydrate aggregates

The dispersion of the hydrate particles formed during each injection was monitored via sonar. As an illustration of the kind of images obtained, a series of three sonar images from injection TO970-4 are presented in Figure 6. The center of each image coincides with the location of the ROV at a depth of 1499.3 m. These images were obtained before the ROV was moved to follow a selected particle as it sank in the water column.

The hydrate aggregates drift away from the injection point and from each other as they sink. In this particular case, the particles spread out in the direction of gravity. As hydrate aggregates slowly dissolve, they become smaller and eventually undetectable by the sonar.

Variations of pH during injections

As shown in Figure 1c, the battery of CJHRs, along with pH probes and thermocouples, was confined in a Plexiglass™ box. The change in pH of the water surrounding the battery of CJHRs was monitored during the injection operations. Figure 7 presents the evolution of pH as injection TO970-4 progresses. The initial "lag" time in pH changes coincides with the start-up period of the reactor. As soon as reaction takes place, there is a drastic decrease of pH from 7.34 to 6.15. Dissolution of unreacted liquid CO_2 is mostly responsible for the sharp decrease in pH. As the reaction progresses and a considerable amount of hydrate aggregates populate the vicinity of the reactors, additional decrease in pH may occur due to the slow dissolution of the occluded liquid

CO_2 from the hydrate aggregates as they slowly drift away from the reactor. The spikes and variations of pH may respond to random movement of newly formed aggregates around the pH probes. When injection stops, the pH returns to the original value as the last aggregates formed drift away from the reactor.

Finally, it should be noted that variations of pH no larger than 1.5 units occur at all times next to the outlet of the CJHRs, where concentrations of unreacted liquid CO_2 and newly formed aggregates are the highest. Lesser effects on the pH of the surrounding water are expected with increasing distance from the reactors, and as the aggregates are dispersed and slowly dissolved.

Plume Modeling

Eric Adams and Aaron Chow

Acknowledgments

Gratefully acknowledged is support by the Ocean Carbon Sequestration Program, Office of Biological and Environmental Research, U.S. Department of Energy, Grant KP1202030, under contract DE-AC05-00OR22725 with UT-Battelle, LLC and contract DE-FG02-01ER63078 with MIT. Support for MBARI was provided by the David and Lucille Packard Foundation and the U.S. Department of Energy under Contract _____. We thank the captain and crew of the RV *Western Flyer* and the pilots of the ROV *Tiburon* for their excellent work in making the field experiments possible. We also thank Dr. C. S. Wong of the Institute of Ocean Sciences of Canada and Dr. P. Bergman of the U.S. Department of Energy for scientific discussions and Dr. Marsha Savage for editing the manuscript.

Literature Cited

(1) Office of Science and Office of Fossil Energy, U.S Department of Energy. *Carbon Sequestration Research and Development*; U.S. Department of Energy Press: Washington, DC, 1999.

(2) Barry, J.; Adams, E.; Bleck, R.; Caldeira, K.; Carman, K.; Erickson, D.; Kennett, J.; McLain, C. Sarmiento, J; Tsouris, C. *Ecosystem and societal consequences of ocean versus atmospheric carbon storage*. Presentation to the American Geophysical Union, San Francisco, CA, December 2005.

(3) Lee, S.Y.; Liang, L.; Riestenberg, D.; West, O.; Tsouris, C.; Adams, E. CO_2 hydrate composite for ocean carbon sequestration, *Environ. Sci. Technol.* **2003**, *37*, 3701–3708.

(4) Tsouris, C; Brewer, C.P.; Peltzer, E.; Waltz, P.; Riestenberg, D.; Liang, L. Hydrate composite particles for ocean sequestration: field verification. *Environ. Sci. Technol.* **2004**, *38*, 1499–1509.

(5) Van der Waals, J. H.; Platteeuw, J. C. Clathrate Solutions. *Adv. Phys. Chem.* **1959**, 2, 1–57.

(6) Sloan Jr., E. D. *Clathrate Hydrates of Natural Gases*, 2nd ed., Marcel Dekker: New York, NY, 1998.

(7) Brewer, P. G.; Friederich, G.; Peltzer, E. T.; Orr Jr., F. M. Direct experiments on the ocean disposal of fossil fuel CO_2. *Science* **1999**, *284*, 943–945.

(8) West, O.R.; Tsouris, C.; Lee, S.; McCallum, S. Negatively buoyant CO_2–hydrate composite for ocean carbon sequestration. *AIChE J.* **2003**, *29*, 276–285.

(9) Riestenberg, D.; Tsouris, C.; Brewer, P.; Peltzer, E.; Walz, P.; Chow, A.; Adams, E. E. Field studies on the formation of sinking CO_2 particles for ocean carbon sequestration:

effects of injector geometry on particle density and dissolution rate and model simulation of plume behavior. *Environ. Sci. Technol.* **2005**, *39*, 7287–7293.

(10) Pacala, S.; Socolow, R. Stabilization wedges: solving the climate problem for the next 50 years with current technologies. *Science* **2004**, *305*, 968–972.

(11) Shindo, Y.; Sakaki, K.; Fujioka, Y.; Komiyama, H. Kinetics of the formation of CO_2 hydrate on the surface of liquid CO_2 droplet in H_2O. *Energy Convers. Manage.* **1996**, *37*, 485–489.

(12) Riestenberg, D.; Chiu, E.; Gborigi, M.; Liang, L.; West, O. R.; Tsouris, C. Investigation of jet breakup and droplet size distribution of liquid CO_2 and H_2O systems — implications for CO_2 hydrate formation for ocean carbon sequestration. *Am. Mineral.* **2004**, *89*, 1240–1246.

(13) Phelps, T. J.; Peters, J.; Marshall, O. R.; West, L.; Blencoe, J. G.; Alexiades, V.; Jacobs, G. K. A new experimental facility for investigating the formation and properties of gas hydrates under simulated seafloor conditions. *Rev. Sci. Instrum.* **2001**, *72*, 1514–1521.

(14) Brewer, P.G.; Peltzer, E.T.; Friedrich, G.; Rehder, E. Experimental determination of the fate of rising CO_2 droplets in seawater. *Environ. Sci. Technol.* **2002**, *36*, 5441–5446.

Tables and Figures

TABLE 1 Jet break up regimes in terms of We number values for the preliminary laboratory experiments and the field experiments discussed in this work.

Experiment	Disp. Phase	Capillary Diameter [mm]	Disp. Phase [l/min]	Cont. Phase [l/min]	H_2O:CO_2	Re	Z	We
Lab 1	CO_2	1.191	5.50*	2.00	3.0	119894	0.0007	7454
Lab 2	CO_2	1.191	5.50*	2.00	3.0	119894	0.0007	7454
Lab 3	CO_2	0.794	5.50*	3.00	4.5	179841	0.0009	25158
Lab 4	CO_2	0.794	5.50*	3.00	4.5	179841	0.0009	25158
Lab 5	H_2O	0.794	3.00	0.66	4.5	6966	0.0126	7725
Lab 6	H_2O	0.794	2.00	0.66	3.0	4644	0.0126	3433
Lab 7	H_2O	1.191	3.00	0.66	4.5	4644	0.0103	2289
Lab 8	H_2O	1.191	2.00	0.66	3.0	3096	0.0103	1017
TO967-2	CO_2	1.191	3.00	7.50	2.5	65397	0.0007	2218
TO967-3	CO_2	1.191	2.50	7.50	3.0	54497	0.0007	1540
TO967-4	CO_2	1.191	2.50	7.50	3.0	54497	0.0007	1540
TO969-1	Seawater	0.794	8.00	1.70	4.7	18576	0.0126	54930
TO969-2	Seawater	0.794	8.00	1.70	4.7	18576	0.0126	54930
TO970-3	Seawater	0.794	3.50	1.50	2.3	8127	0.0126	10514
TO970-4	Seawater	0.794	3.75	1.50	2.5	8707	0.0126	12070
TO970-6	Seawater	0.794	3.50	1.50	2.3	8127	0.0126	10514

* Flowrate corrected to account for the pulsed flow obtained from the CO_2 pump used in laboratory experiments.

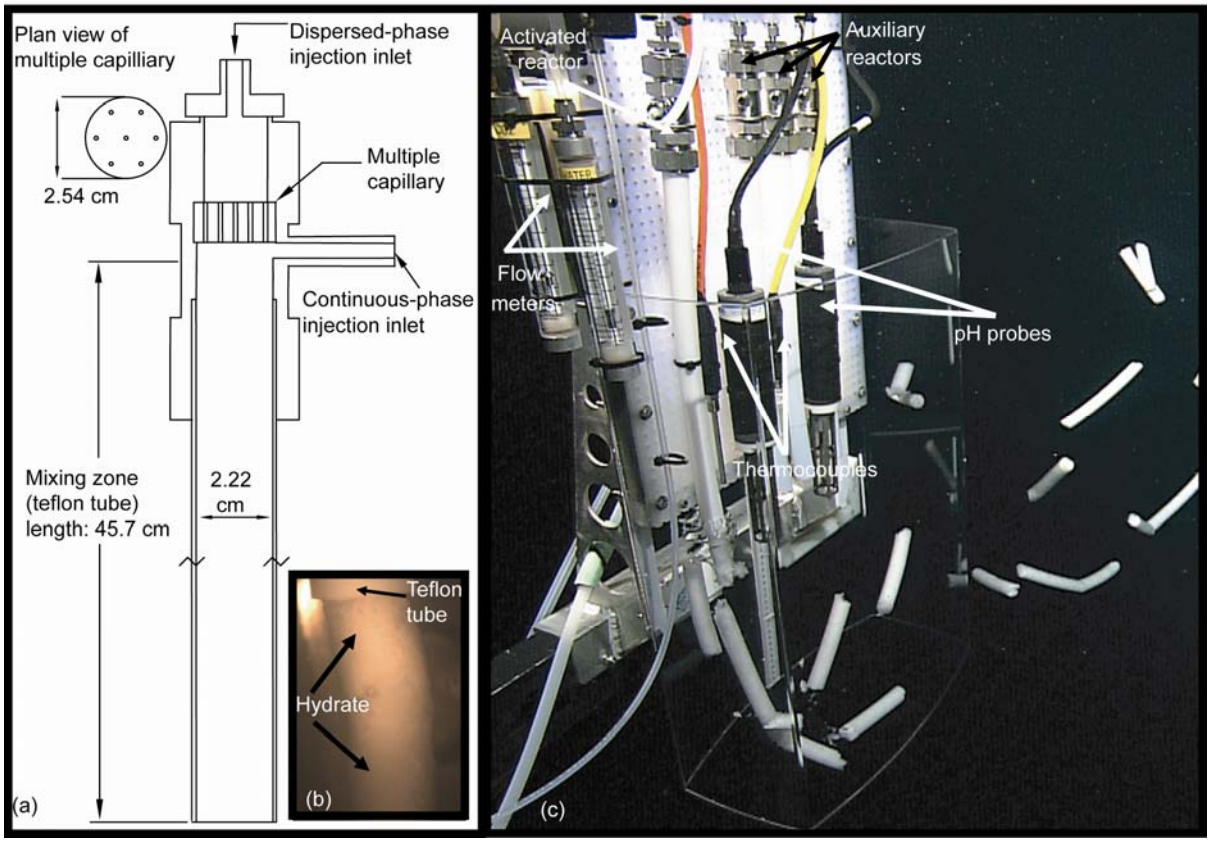

FIGURE 1 (a) Schematic of the pilot-scale CJHR reactor utilized in preliminary laboratory experiments and field experiments. (b) Close-up picture of hydrate particles exiting the mixing zone of the CJHR reactor during laboratory experiments. (c) Picture of the experimental set up for the field experiments, mounted on the ROV *Tiburon*.

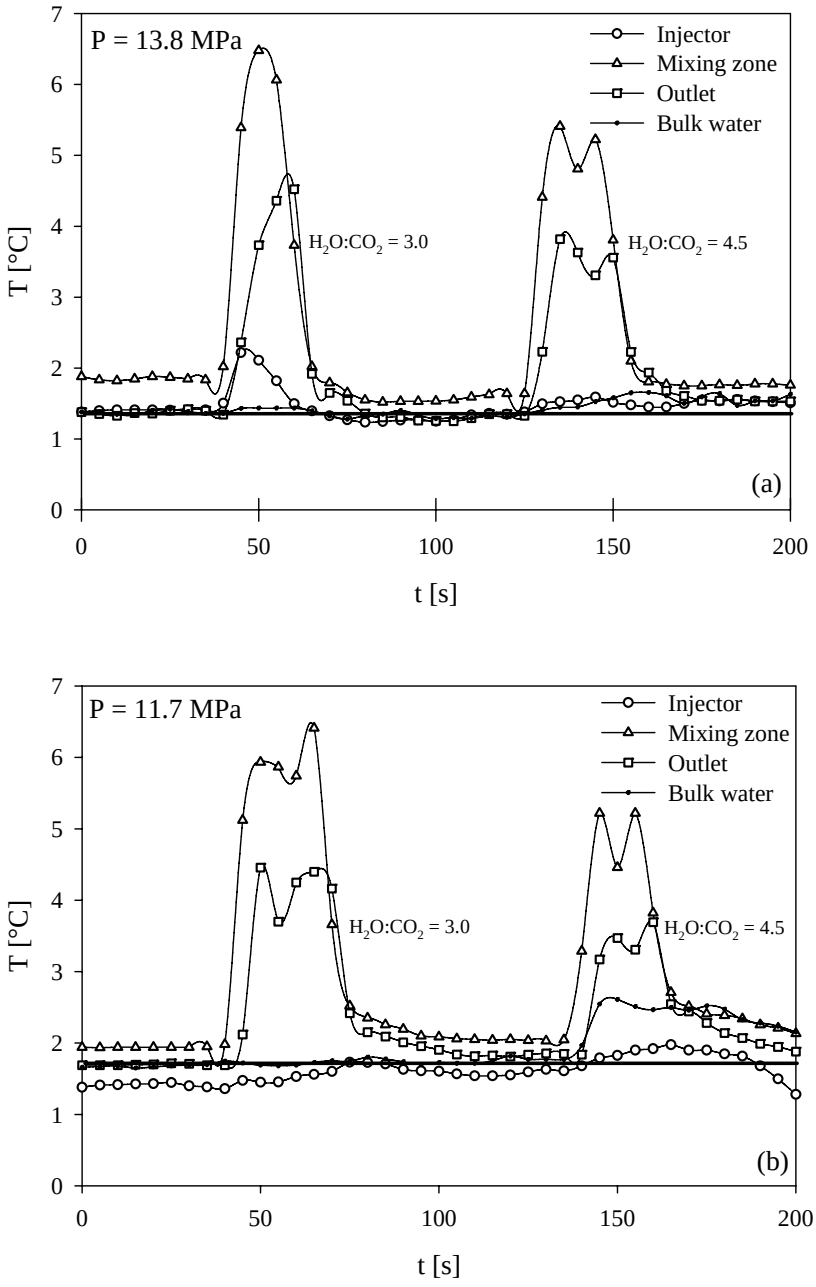

FIGURE 2 Temperature profiles (i.e., temperature vs. time of injection) for laboratory experiments (a) at P = 13.8 MPa, and (b) at P = 11.8 MPa.

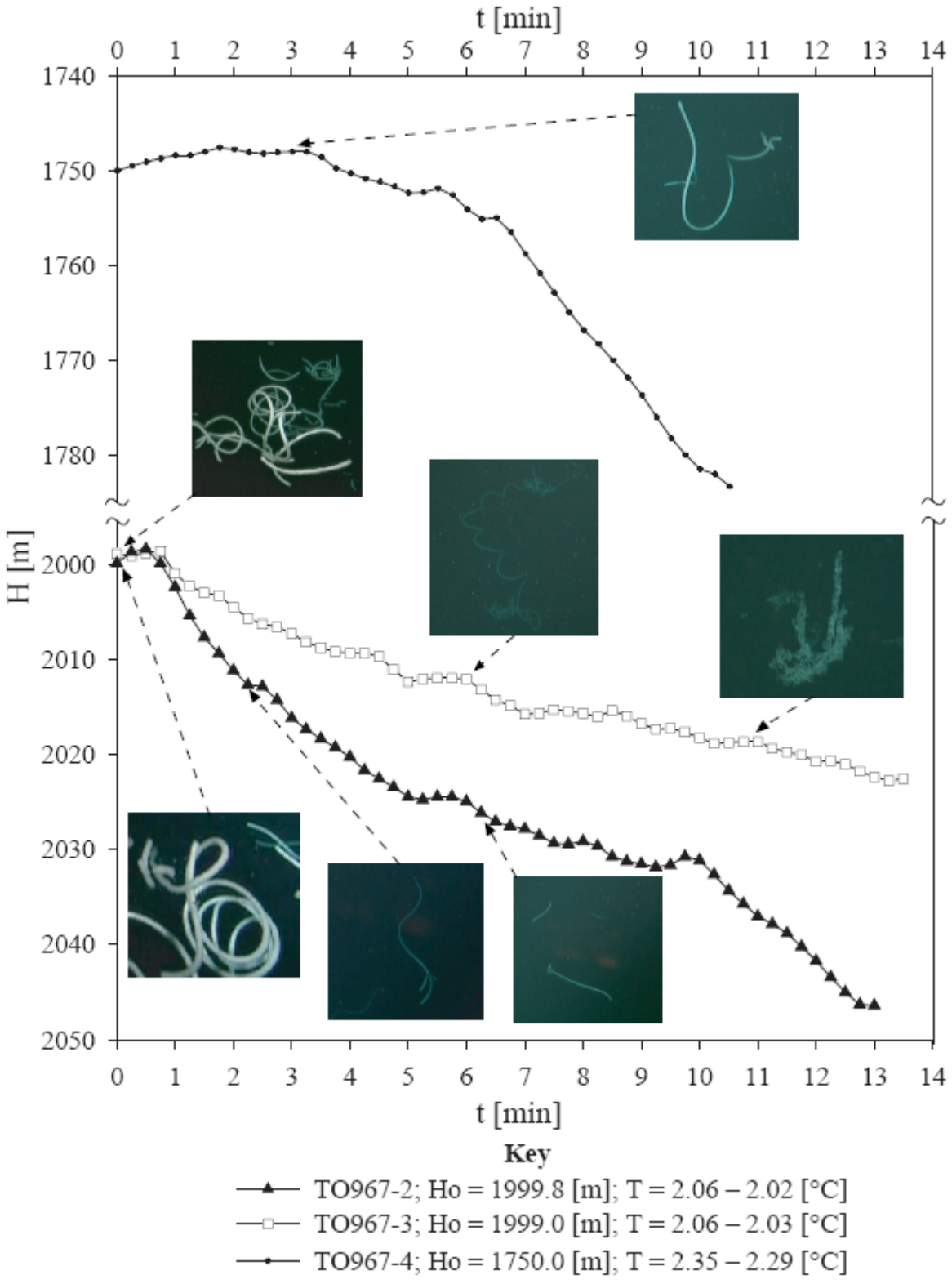

FIGURE 3 Depth vs. time profiles (vertical movement) of CO_2-hydrate aggregates produced during experiments TO967, with CO_2 as the dispersed phase.

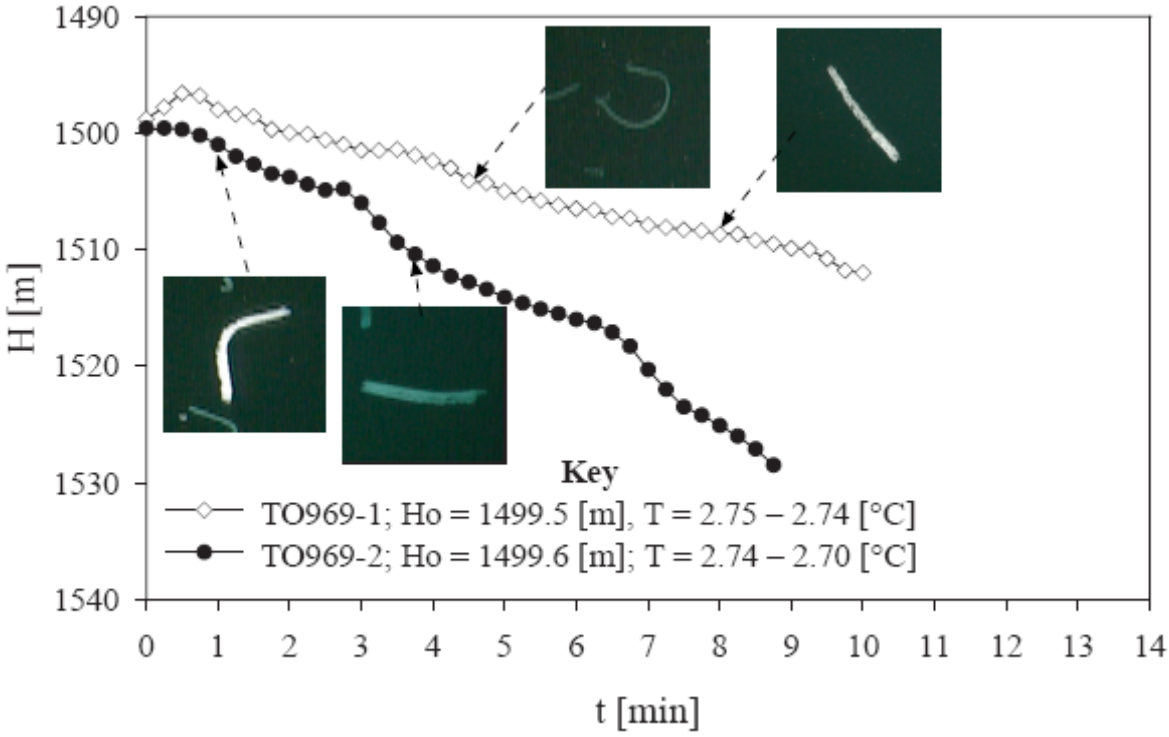

FIGURE 4 Depth vs. time profiles (vertical movement) of CO_2-hydrate aggregates produced during experiments TO969, with H_2O as the dispersed phase.

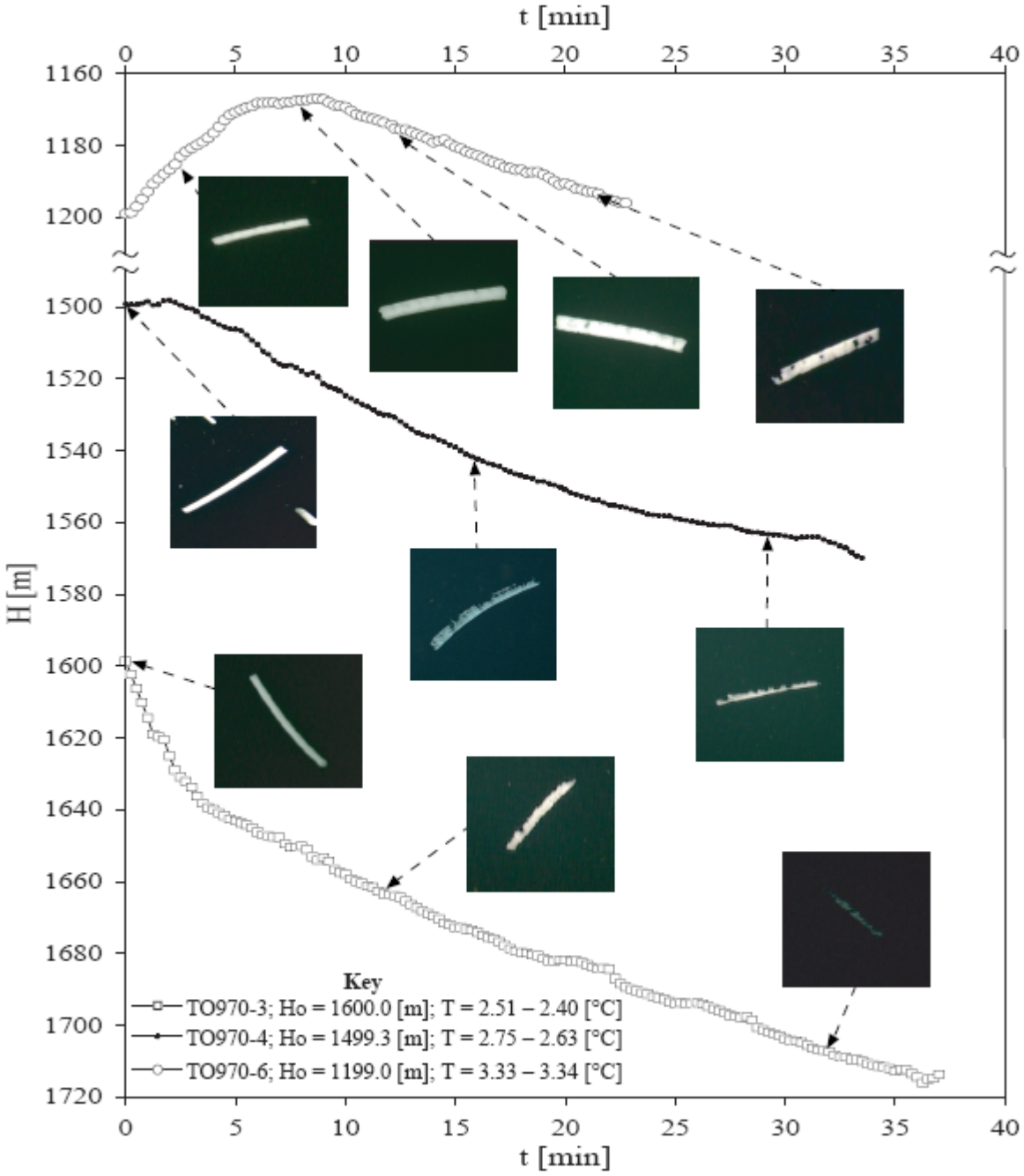

FIGURE 5 Depth vs. time profiles of CO_2-hydrate aggregates produced during experiments TO970, with H_2O as the dispersed phase.

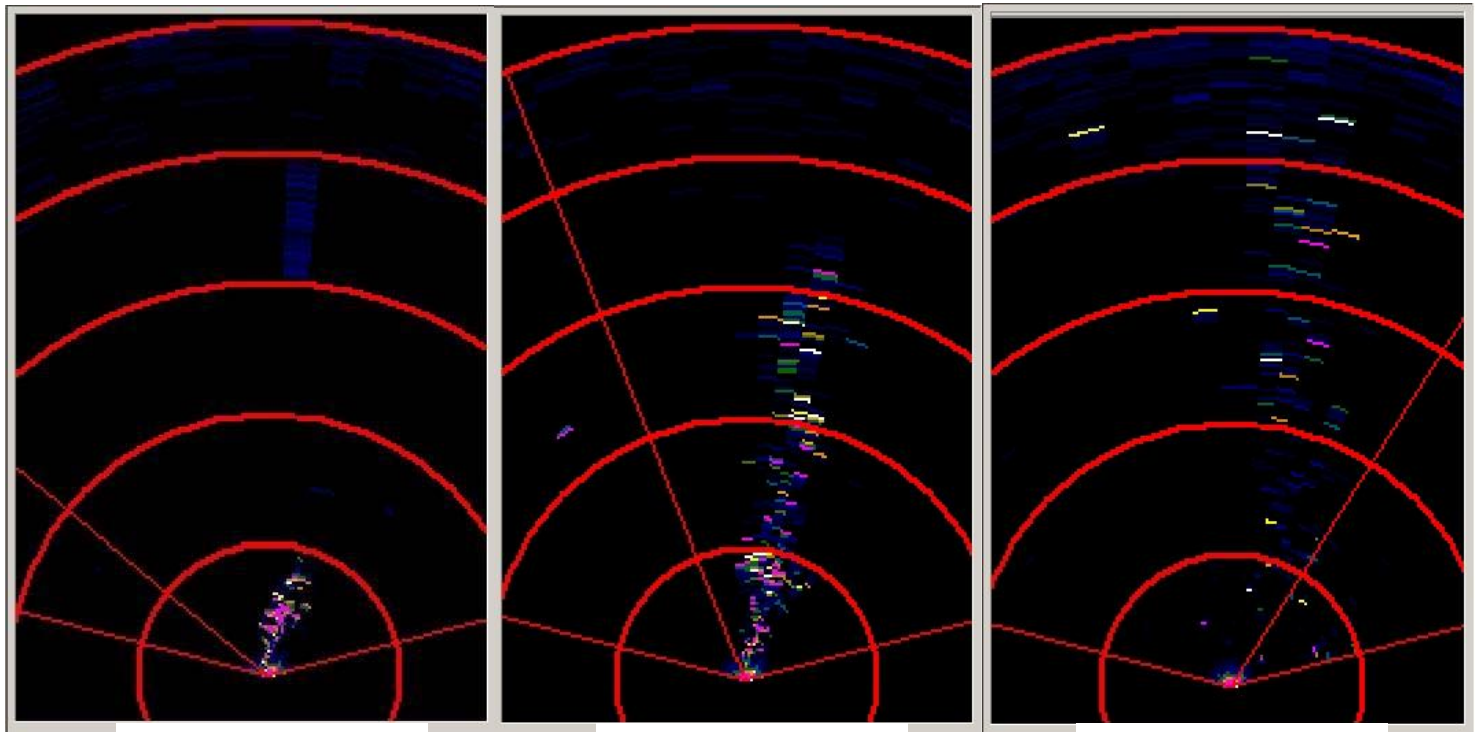

FIGURE 6 Sonar images obtained during field injection TO970-4 at a depth of 1499.3 m. Scale: 8 m/division.

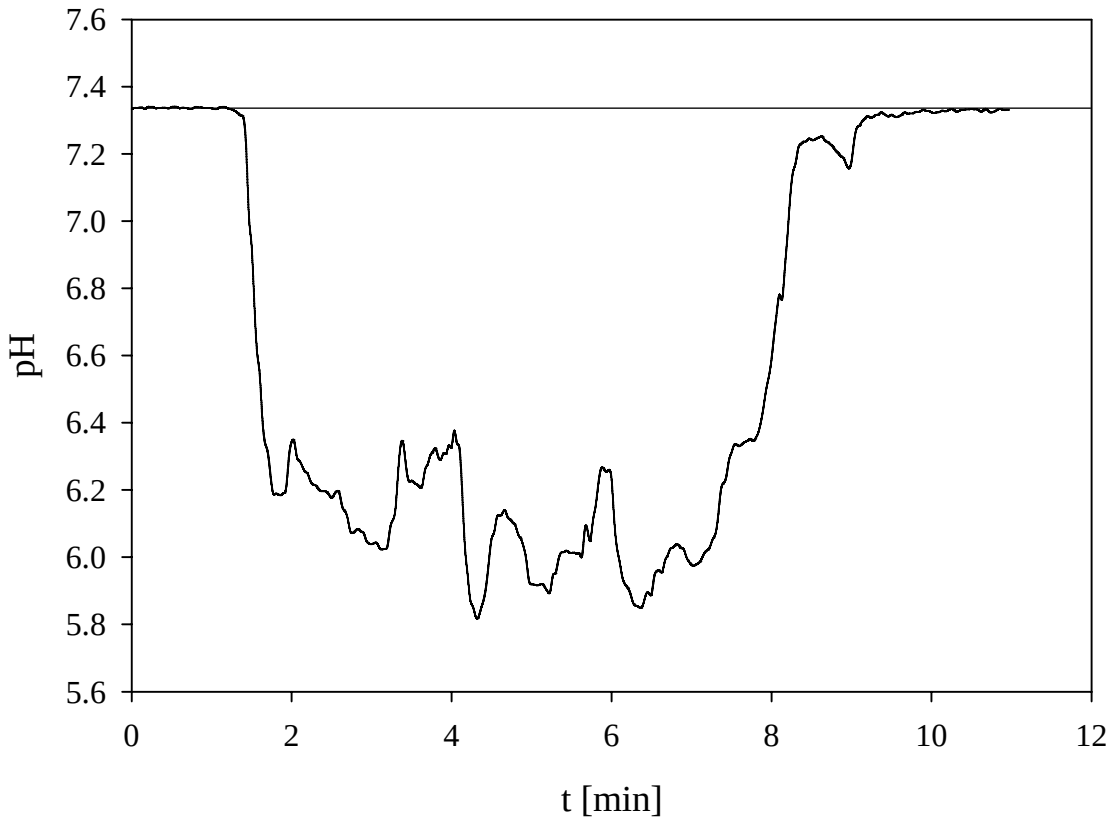

FIGURE 7 Variation of pH vs. injection time recorded during field injection TO970-4.

An *in situ* oceanic experiment on the exchange reaction between liquid CO_2 and a natural gas hydrate: A feasibility test

August 29, 2006

Introduction

The question of whether the conversion of methane hydrate to CO_2 hydrate can be achieved by simply bathing a methane hydrate mass in liquid CO_2, with the release of methane gas and the sequestration in solid form of the introduced CO_2 is of considerable current interest. If such a reaction can be achieved it offers in principle a way of sequestering captured fossil fuel CO_2 within a geologic reservoir, with the recovery of methane gas as an additional energy source. The thermodynamic arguments in favor of this rest on the difference in free energy for the two hydrate states. Simply put the enthalpy changes occurring on hydrate formation are a function of the hydrate cavity occupation, and thus if a CO_2 molecule can more easily (less energy required) occupy the large cage of a $5^{12}6^2$ Structure I hydrate than can CH_4 then the replacement is favored with the liberation of a small amount of heat. The above argument rests upon classical thermodynamic grounds and has long attracted researchers as a theoretical possibility. But such arguments ignore energy barriers for the transition, and say nothing of the rate at which the exchange can proceed. Nor do they address the typical problem of build-up of reaction products at the interface thus providing a diffusive barrier separating the reacting species. Nonetheless there is intense interest in this topic, and progress has been made in assessing the possibilities.

Background

Recently several researchers have explored this reaction in a series of laboratory studies. The properties of many gas hydrates are given in the text by Sloan (1998); the properties of CO_2 hydrates have been carefully documented by Ohgaki et al. (1993). Komai et al. (2002) carried out laboratory observations of the exchange behavior in a small pressure cell by Raman spectroscopy. They reported slow conversion rates (several hours) with the rate markedly increasing as the temperature approached the formation point of liquid water. Lee et al. (2003) carried out a similar laboratory study on finely ground hydrates to increase the surface area for reaction, and with the use of ^{13}C NMR to investigate the details of cage occupancy. They reported that when CH_4 hydrate was exposed to CO_2 gas the guest replacement was complete in less than 5 hours, and that the CH_4 obtained from the reaction was about half the CH_4 present in the initial hydrate. Park et al. (2006) examined the use of a CO_2-N_2 mixture as a reactant, and reported that this markedly increased the CH_4 yield since the N_2 gas could occupy the small cages in the hydrate structure. Graue et al. (2006) reported the first example of CH_4 displacement from hydrate resident within a porous medium (sandstone) by using NMR imaging to detect the exchange process.

All of the above experiments are laboratory studies; so far as we are aware no field experiments have yet been carried out. Such studies present quite difficult challenges; the temperature and pressure conditions are set by the external environment, and typically CO_2 will be in the liquid state. Many of the observing tools used in laboratory studies are not available for deep-ocean or deep-earth observations, and, if

they are, are controllable only with difficulty. Natural samples of hydrate, and their sedimentary surroundings, are strongly fluorescent, thus posing challenges for optical techniques. The hydrates encountered in nature may be macroscopic, with far less area for reaction than the finely ground material used in laboratory studies. The laboratory experiments above have exclusively used pure Structure I methane hydrates, and many thermogenic Structure II hydrates occur in nature, with quite different P-T stability fields. And field equipment is expensive, so that long data acquisition times require special consideration. Yet unless the laboratory interests can be transferred to controlled field studies and operate on the macroscopic scale, with all the complexity that implies, the subject is likely to remain only of academic interest.

Previous Work

In earlier work we have assembled many of the tools required for carrying out such field experiments, albeit with difficulty. We have developed an in situ laser Raman spectrometer for deep ocean work (Brewer et al., 2004; Pasteris et al., 2004), and used this to examine the cage occupancy of both experimentally created (Hester et al., 2006a) and natural gas hydrates (Hester et al., 2006b). We have developed techniques for safely containing, transporting, and injecting liquid CO_2 in the deep ocean (Brewer et al., 1999) and for observing it's reaction rate with the surrounding sea water (Brewer et al., 2005; Dunk et al., 2005). Thus we have the opportunity for combining these skills to examine in the field the possible CO_2-CH_4 hydrate exchange reactions described above.

Field work

We have carried out a simple short term field experiment on the CO_2-natural gas hydrate reaction to explore technique and guide future work at the massive thermogenic gas hydrate exposure site at 850m depth at Barkley Canyon, offshore Vancouver Island (Chapman et al., 2004; Pohlman et al., 2005). The experiment took place August 15-17, 2006.

The essential tool for deploying and controlling these systems in the deep-sea is a fully developed remotely operated vehicle (ROV) and we have used the ROV Tiburon for this work. The site was located at 48° 18.642'N 126° 3.903'W. A hydrate sample was obtained by using a small stainless steel coring tool held in the vehicle arm, and using an approximately 270° repetitive rotating motion to obtain an approximately 10 cm x 4 cm core (Figure 1). Coring was achieved only with difficulty for the hydrate surface was extraordinarily hard to penetrate. Durham et al. (2003) measured the strength and rheology of a pure methane hydrate, and reported it to be over 20x stronger than water ice. The strength of a Structure II hydrate, such as that observed here, has not been measured but our experience suggests that it is comparable.

Figure 1. *Coring an exposed yellow oil stained hydrate surface at Barkley Canyon on 08/15/2006. The core diameter is approximately 4 cm.*

The recovered core was then expelled by a hydraulic ram into a glass chamber held on the vehicle, where it floated to the top. A second hydrate core was similarly obtained and injected. A dispensing nozzle was then acquired and approximately 2 L liquid CO_2 carefully dispensed into the experimental chamber; at these depths liquid CO_2 is also less dense than sea water, however the densities of the CO_2 and the hydrate are closely matched and there was some prior uncertainty as to their relative buoyancies. In practice the hydrate remained floating at the top of the chamber, and was fully bathed in liquid CO_2 (Figure 2).

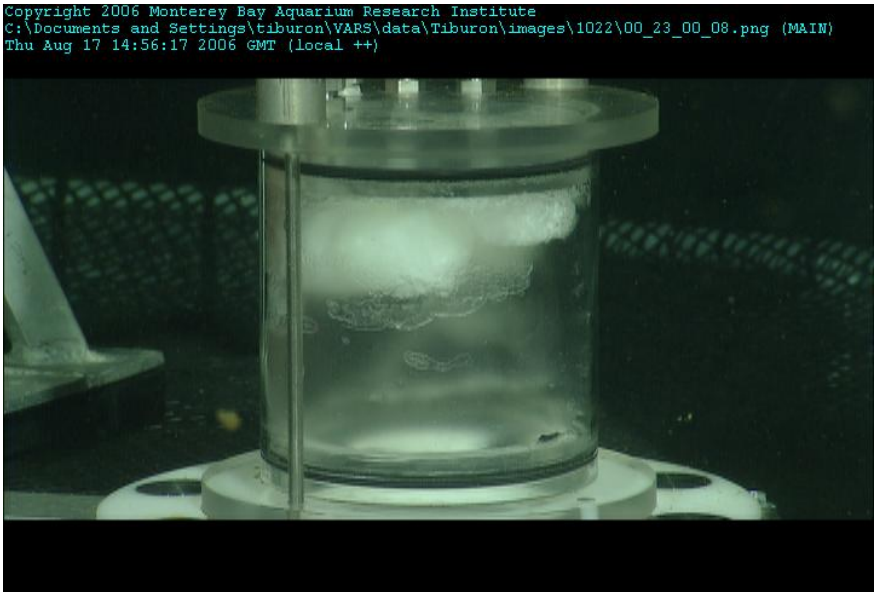

Figure 2. *The glass chamber containing about 2 L liquid CO_2. The two cores of a white hydrate are seen floating at the top of the chamber, which has been placed on a flat*

aluminum plate to cut off dissolution of the CO_2 into the surrounding ocean water. The thin frosting of CO_2 hydrate on the inner wall of the chamber results from incomplete drainage of the water film on the glass surface.

The sample chamber was first placed on a flat aluminum plate to close off the bottom surface, and then closely inspected with the ROV HDTV camera. The system was then left for approximately 48 hours, with periodic visual inspection, and then examined by in situ laser Raman techniques on 08/17/2006 to investigate possible reaction progress. For this the chamber was carefully removed from the base plate, and transferred to a Precision Underwater Positioner (PUP) system for precise control of the laser beam (White et al., 2005). By means of this system we were able to scan with sub-millimeter precision around the system, and by controlled focusing of the laser beam acquire spectroscopic data on the free liquid CO_2, the solid hydrate, and by careful stepping of the focal point the hydrate boundary layer where any reaction products may be expected to occur.

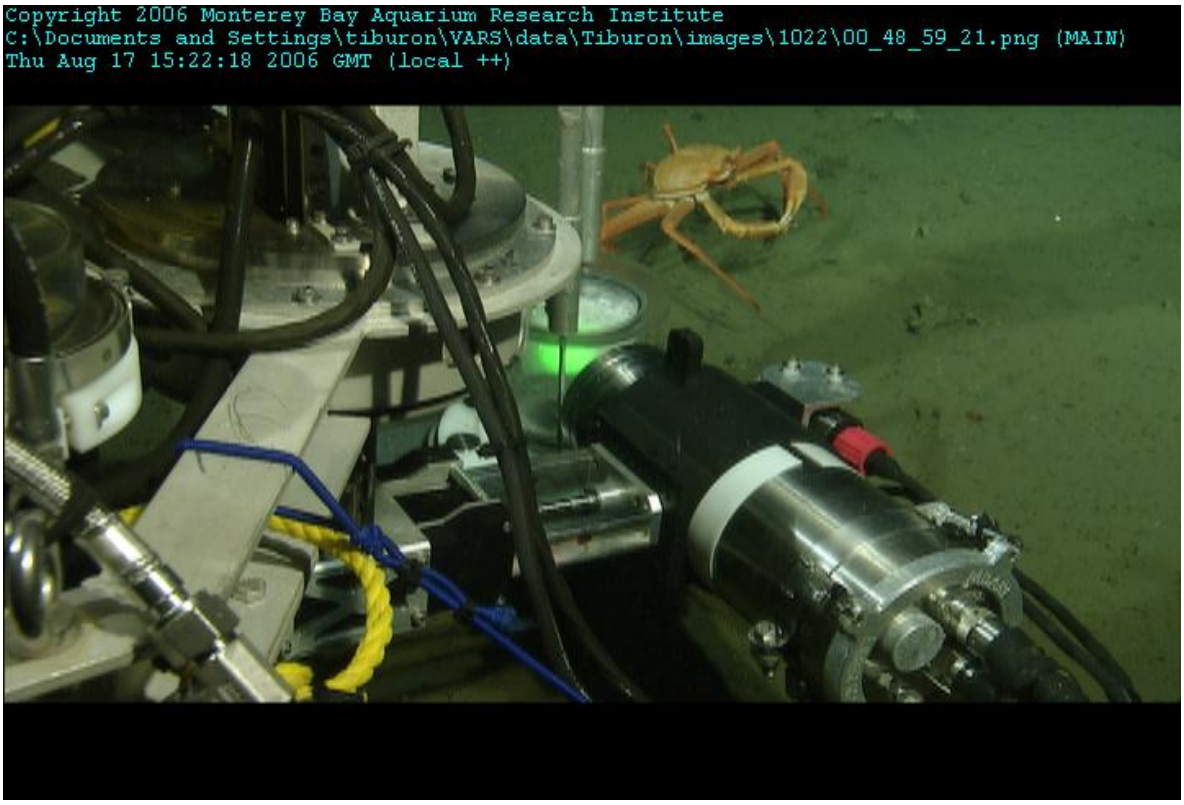

Figure 3. *The laser probe head mounted on the Precision Underwater Positioner (PUP) interrogating the CH_4 hydrate-liquid CO_2 exchange experiment chamber at 850m ocean depth. The head can be scanned in 3-dimensions with sub-millimeter precision.*

Results

The results obtained are best seen by reference to Figure 4, in which data from the CO_2 region and the C-H region of the same spectra are clipped and compared. Each file

represents a distinct focal point of the laser as the mass of liquid and solid was explored in three dimensions.

All spectra have been baseline corrected to remove broad fluorescence interference resulting from traces of oil occurring in the sample. The spectra have also been treated to remove the well known water signal, which has the largest effect at wave numbers slightly higher than the C-H stretching bands. The fluorescence signal was most pronounced in File 7, where it was strong enough to swamp the diamond calibration peak present in all spectra (Brewer et al., 2004).

Our selection of spectra and choice of where to focus the laser was based upon the need to explore all phases – liquid CO_2, solid hydrate, any created CO_2 hydrate, and any liberated methane gas. We were to some degree successful in all of this. In File 2 of Figure 4 we show the presence of dissolved CH_4 (right panel) within the bulk liquid CO_2 (left panel). The solubility of CH_4 in CO_2 is significant, and we may not expect liberation of a free CH_4 gas phase until the saturation condition has been met. So strong is the response of the liquid CO_2 that it swamps the small diamond signal seen between the Fermi dyad of the CO_2 peaks; nonetheless the diamond signal still provides an accurate spectral reference. The small dissolved CH_4 peak is shown on an x50 expanded scale, but it is spectrally distinct from the source solid hydrate.

File 7 of Figure 4 records the primary hydrate signal. High fluorescence in this sample resulted in only short acquisition times before the detector was saturated and thus the baseline is noisy. The hydrate contains CH_4, C_2H_6, and C_3H_8 and these bands are visible.

File 4 shows the presence of commingled CO_2 hydrate and CH_4 hydrate occurring at the interface between solid and liquid. The CO_2 hydrate peaks are distinguishable from the liquid, but they are small and the diamond peak between the pair is relatively large in this spectrum. The right panel shows the presence of methane hydrate, apparently without the C_2H_6 contribution seen in File 7. The co-existence of these forms here hints at the process that may be at work.

In File 5 we record the presence of free methane gas in a small but visually identifiable bubble layer at the top of the chamber. The C-H signal clearly identifies the gas signature; the CO_2 region is devoid of peaks since CO_2 is in the liquid state and its vapor pressure is low in the trapped CH_4 gas phase.

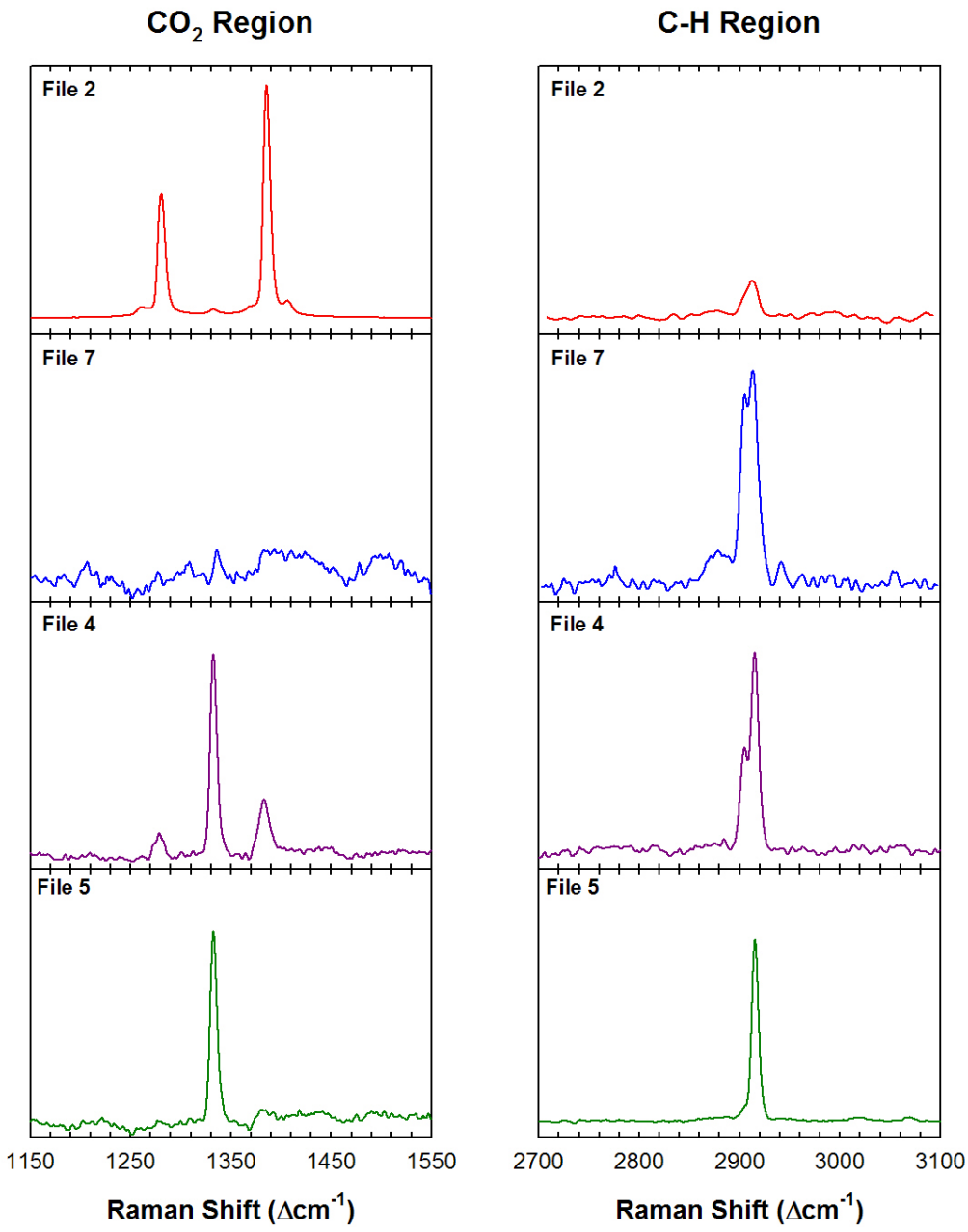

Figure 4. *Spectra obtained of: Dissolved CH_4 in liquid CO_2 (File 2), the primary Structure II hydrate (File 7), commingled CO_2 and CH_4 hydrate (File 4), and liberated CH_4 gas accumulated at the top of the chamber (File 5).*

Discussion

The results described above provide a tantalizing hint of processes that may be at work. It must be stressed that this experiment was carried out to explore procedure, and to examine whether the unique ensemble of protocols required could be successfully combined in a field setting, and whether reasonable results could be obtained with such a relatively large scale small surface area system.

It must first be pointed out that the choice of a complex Structure II thermogenic gas hydrate was dictated simply by availability and not by thermodynamic argument; the experiment was opportunistically carried out as adjunct to an expeditionary geochemical study of a major natural hydrate exposure site. There may well be some doubt as to the thermodynamic basis for the reaction proceeding: for example under typical northeast Pacific ocean conditions the phase boundary for CH_4 hydrate formation occurs at about 550m depth. The phase boundary for formation of CO_2 hydrate occurs at about 350m depth. The phase boundary for formation/decomposition of the complex thermogenic hydrate used here is at approximately 200m depth – so purely on the basis of the P-T field stability of the bulk material the displacement of CH_4 by CO_2 may not be favored since the ethane present may confer greater stability. A full thermodynamic assessment could yield a more sophisticated answer, but the simple P-T argument is usefully illustrative.

If the entire hydrate system is homogeneous and cage occupancy is 100% then we may suspect on thermodynamic grounds that very little CO_2 should be accommodated; however if a mixed Type I and II hydrate structure is present then substitution could occur. There is also evidence at this site of trace quantities of Structure H hydrate accommodating yet larger molecules such as n-pentane and n-hexane (Lu et al., 2006).

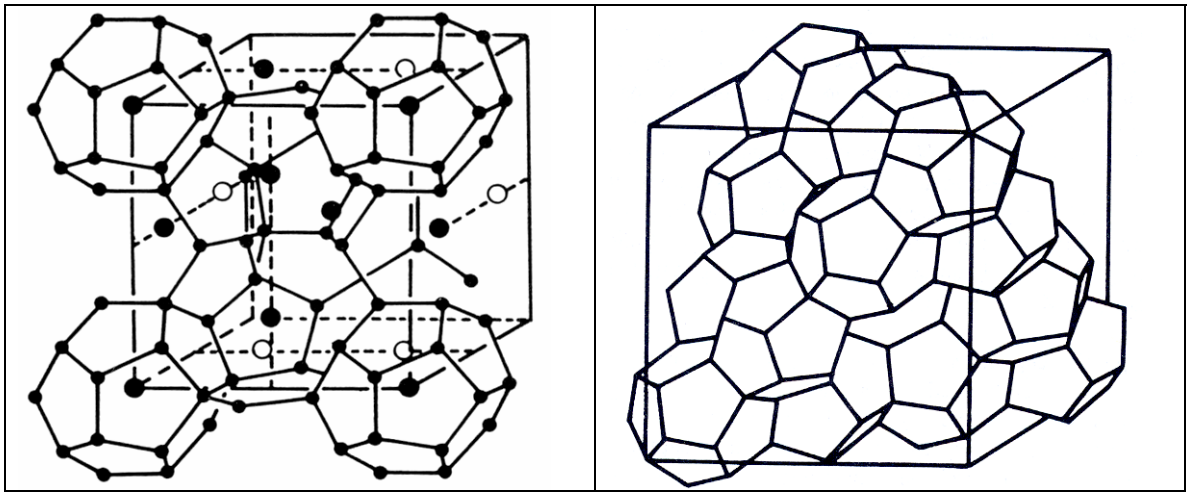

Figure 5. *Unit cell structures of a Type I $5^{12}6^2$ hydrate (left), and a type II $5^{12}6^4$ hydrate (right); the Type II structure defines the hydrates investigated here. From Sloan (1998).*

Gas hydrates are non-stoichiometric compounds, and only rarely in nature does full cage occupancy occur. Thus even a dense Structure II hydrate such as this may have large cage vacancies that can accommodate the CO_2 molecule; Lu et al. (2006) report that "about 80% of the water was in the hydrate phase" suggesting that some vacancies were indeed present in a sample from this site.

Secondly, although no signal of free methane gas trapped in the original hydrate was seen spectroscopically, the area observed by this means is small and some free methane gas originally present may possibly be have been released in the CO_2 bath, and thus not originate from a true displacement reaction.

The addition of liquid CO_2 to the chamber displaces water, and a CO_2 hydrate film is formed at the interfaces – very likely including that at the cored hydrate-liquid CO_2 contact surface – without any associated CH_4 exchange. The wet glass surface through which spectra are obtained was also seen to have a thin CO_2 hydrate film through which the unfocused part of the laser beam must pass.

The time scale for the experiment was limited by practical expedition concerns, and not matched to any observed or predicted rates, nor was any effort made to increase the surface area for reaction. Thus the time for initial saturation of the large volume of liquid CO_2 may have been considerable, and the small free gas presence we observed may have originated only in the last few hours before spectroscopic examination.

The spectral separation of the free and hydrate forms of the major components is not large, and while well recognizable in laboratory studies the signals require careful assessment under more robust expedition conditions. As an example of this we show the results for the simultaneous detection of liquid CO_2 and CO_2 hydrate (Figure 6); the shift is only 2 cm^{-1} from liquid to hydrate state with the hydrate form exhibiting a lower Raman shift.

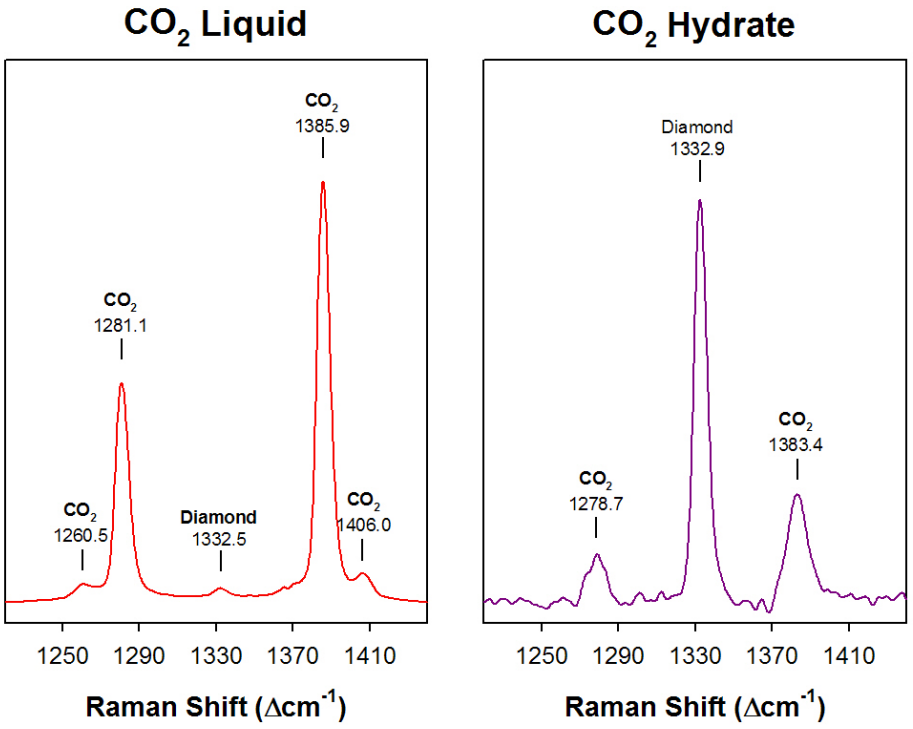

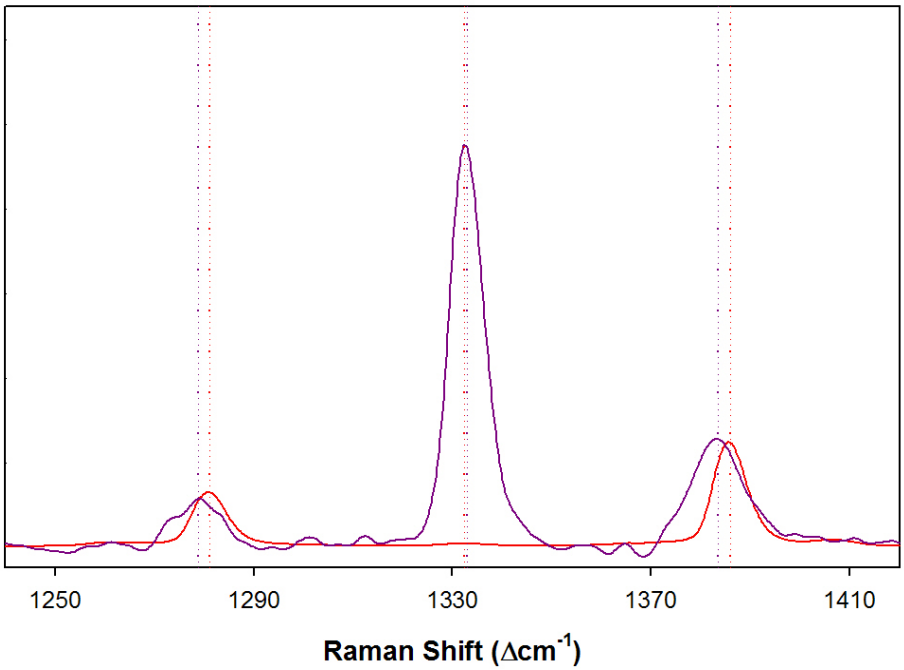

Figure 6. *Upper Panel: The Raman spectra of liquid CO_2 and CO_2 hydrate obtained with our system at depth. Note that the peak intensities are very different as seen by the relative strength of the diamond standard, but that peak wave number is identified with the same accuracy.*

Lower Panel: The overlain plot of the liquid and hydrate spectra with the CO2 peaks scaled to the same height to aid comparison of peak position.

Conclusions and Further Work

We conclude that controlled sea floor experiments on the possible sequestration of CO_2 and the liberation of CH_4 are possible with existing techniques, and on a time scale of days, even with bulk material of relatively small surface area. The use of a complex Structure II hydrate is decidedly non-ideal, and was dictated here only by opportunistic access to this site. Care must be taken to avoid artifacts, such as formation of CO_2 hydrate simply during the liquid introduction process, and hydrate frosting on the glass container surface. These problems have already been overcome in the work of Dunk et al. (2005) in which the reaction vessel was plumbed so that liquid CO_2 was slowly introduced through the upper lid of the container, thereby avoiding turbulence and effectively displacing droplets from the walls so that a frost-free surface was available. It was not possible to assemble all these features in the preliminary experiment reported here, but this could easily be done for future work.

So far as we are aware the limits set by the finite solubility of CH_4 in liquid CO_2 have not been discussed in previous work, yet this is readily calculable. In a true field test it would be difficult to control the liquid CO_2 to CH_4 hydrate ratio, and if a large excess of CO_2 is present then it may be that simple dissolution of CH_4 is all that is seen.

The rate of reaction observed by us here, and by others, suggests that rates far above simple diffusion are occurring, and this must be so if any active process of

substitution of the hydrate with gas release is to take place. There are no well defined explanations for this, but we point out that while the bulk hydrate structures are known with very high precision, knowledge of the hydrate-water interface, where partial cage structures should occur, is very limited. We have observed that the marked density contrasts resulting from formation of dense CO_2 saturated aqueous boundary layers can produce dramatic fluid dynamic effects (Brewer et al., 1999) with rapid overturning of the bulk fluid. It may be that such density driven boundary layer effects play an important role in controlling the surface renewal rates required here.

Acknowledgments

We thank all the talented people at MBARI who created and tested the complex systems used in carrying out this work. The experiments would not have been possible without the skilled support of the crew of the RV Western Flyer, and in particular the pilots of the ROV Tiburon who superbly executed the manipulations required.

The work was supported by a grant to MBARI by the David and Lucile Packard Foundation, the National Undersea Research Program of NOAA, and the U.S. Dept. of Energy Grant No. DE-FC26-00NT4092.

References

Brewer, P.G., G. Friederich, E.T. Peltzer, and F.M. Orr, Jr. (1999) Direct Experiments on the Ocean Disposal of Fossil Fuel CO_2. *Science*, **284**, 943-945.

Brewer, P.G., Malby, G., Pasteris, J.D., White, S.N., Peltzer, E.T., Wopenka, B., Freeman, J., and Brown, M.O. (2004) Development of a laser Raman spectrometer for deep-ocean science. *Deep-Sea Res.* I, **51**, 739-753.

Brewer, P.G., E.T. Peltzer, P. Walz, I. Aya, K. Yamane, R. Kojima, Y. Nakajima, N. Nakayama, P. Haugan, and T. Johannessen (2005) Deep Ocean Experiments with fossil fuel carbon dioxide: creation and sensing of a controlled plume at 4 km depth. *J. Mar. Res.*, **63**, 9-33.

Chapman,R., J. Pohlman, R. Coffin,J. Chanton, L. Lapham (2004) Thermogenic gas hydrates in the northern Cascadia margin. *Eos, Trans. Am. Geophys., Union*, **85**, 361-368.

Dunk, R.M., E.T. Peltzer, P. Walz, and P.G. Brewer (2005) Seeing a Deep Ocean CO_2 Enrichment Experiment in a New Light: Laser Raman Detection of Dissolved CO_2 in Seawater. *Environ. Sci. Technol.*, **39**, 9630-9636.

Durham, W.B., S. H. Kirby, L.A. Stern, and W. Zhang (2003) The strength and rheology of methane clathrate hydrate. *J. Geophys. Res.*, **108**, doi:10.1029/2002JB001872.

Graue, A., B. Kvamme, B.A. Baldwin, J. Stevens, J. Howard, E. Aspenes, G. Ersland, J. Husebo, and D.R. Zornes (2006) Environmentally friendly CO_2 storage in hydrate reservoirs: Benefits from associated spontaneous methane production. Offshore Technology Conference, 2006.

Hester, K.C., S.N. White, E.T. Peltzer, P.G. Brewer, and E.D. Sloan (2006) Raman spectroscopic measurements of synthetic gas hydrates in the ocean. *Mar. Chem.*, **98**, 304-314.

K.C. Hester, S.N. White, R.M. Dunk, P.G. Brewer, E.T. Peltzer, and E.D. Sloan (2006) In situ gas hydrate measurements at Hydrate Ridge using Raman spectroscopy. *Geochim. Cosmochim. Acta.* Submitted.

Komai, T., T. Kawamura, S. Kang, K. Nagashima, and Y. Yamamoto (2002) In situ observation of gas hydrate behavior under high pressure by Raman spectroscopy. *J. Phys. Condes. Matter*, **14**, 11395-11400.

Lee, H., Y. Seo, Y.-T. Seo, I. L. Moudrakovski, and J. A. Ripmeester (2003) Recovering methane from solid methane hydrate with carbon dioxide. *Angew. Chem. Int. Ed.*, **42**, 5048-5051.

Lu, H., Y.-T. Seo, J.-W.Lee, I. Moudrakovski, J. Ripmeester, N.R. Chapman, R.B. Coffin, G. Gardner, and J. Pohlman (2006) Complex gas hydrate from the Cascadia margin. In preparation.

Ohgaki, Y. Y. Makihara and K. Takano (1993) Formation of CO_2 hydrate in pure and sea waters. *J. Chem. Eng. Jpn.*, **26**, 558-564.

Park, Y., D.-Y. Kim, H. Lee, J.-W Lee, D.-G. Huh, K.-P. Park and J. Lee (2006) Sequestering carbon dioxide into complex structures of naturally-occurring gas hydrates. *Proc. Natl. Acad. Sci*., In Press.

Pasteris, J.D., B. Wopenka, J.J. Freeman, P.G. Brewer, S.N. White, E.T. Peltzer, and G. Malby. (2004) Raman spectroscopy in the deep ocean: Successes and challenges. *Applied Spectroscopy*, **58 (7)**, 195A – 208A.

Pohlman, J.W., E.A. Canuel, N. R. Chapman, G.D. Spence, M.J. Whiticar, and R.B. Coffin (2005) The origin of thermogenic gas hydrates on the northern Cascadia margin as inferred from isotopic ($^{13}C/^{12}C$ and D/H) and molecular composition of hydrate and vent gas. *Organic Geochem.*, **36**, 703-716.

Sloan, E.D. (1998) Clathrate hydrates of natural gases. Marcel Dekker, 705 pp.

White, S.N.. Kirkwood, W., Sherman, A., Brown, M., Henthorn, R., Salamy, K., Walz, P., Peltzer, E.T., and Brewer, P.G. (2005). Development and deployment of a precision underwater positioning system for in situ laser Raman spectroscopy in the deep ocean. *Deep-Sea Res*. I, **52**, 2376-2389.